

The Sound of Sonoluminescence

H.-Thomas Elze^{1,2}, Takeshi Kodama² and Johann Rafelski¹

¹Department of Physics, University of Arizona, Tucson, AZ 85721

and

²Universidade Federal do Rio de Janeiro, Instituto de Física
Caixa Postal 68.528, 21945-970 Rio de Janeiro, RJ, Brazil

August 10, 1997

Abstract

We consider an air bubble in water under conditions of single bubble sonoluminescence (SBSL) and evaluate the emitted sound field nonperturbatively for subsonic gas-liquid interface motion. Sound emission being the dominant damping mechanism, we also implement the nonperturbative sound damping in the Rayleigh-Plesset equation for the interface motion. We evaluate numerically the sound pulse emitted during bubble collapse and compare the nonperturbative and perturbative results, showing that the usual perturbative description leads to an overestimate of the maximal surface velocity and maximal sound pressure. The radius vs. time relation for a full SBSL cycle remains deceptively unaffected.

43.28.R, 43.35.+d, 47.10.+g, 47.35.+i, 47.55.Bx, 47.55.Dz, 68.10.-m

1 Introduction

This extensive study of the sound produced in single bubble cavitation is prompted by the recent interest in sonoluminescence (SL), i.e. the conversion of externally applied sound in a liquid into light [1]. It has been generally accepted that the SL light emission is intimately connected to the dynamics of the gas-liquid interface, though the specific mechanism producing the light flashes has not been uniquely identified. We present here a nonperturbative study of the sound radiated from the subsonically moving phase boundary between the gas bubble and the liquid in which it is immersed. In our approach we rely on the standard treatise of the subject [2]. Apart from the importance of sound emission as the primary damping mechanism under the extreme conditions of sonoluminescence, the sound signal can be used as another diagnostic tool to study the bubble dynamics. For detailed accounts of related previous theoretical studies of the cavitation sound see Refs.[3, 4], including references to earlier work. We proceed here in two distinct steps:

- To begin with, the motion of the gas-liquid phase boundary is assumed to be given and we determine the resulting sound field.
- Secondly, we consider the feedback effect of the radiated sound field onto the phase boundary dynamics, i.e. we describe the motion of the bubble selfconsistently.

The (multi-)bubble cavitation has been studied intensely for some time, because of important applications and interesting underlying fluid dynamics [5, 6, 7]. The discovery of well controlled

experimental conditions by Gaitan and Crum [8] permitting the study of a single gas bubble over long periods of time, together with the ability to drive it externally by acoustic waves, has focused the experimental interest on the single bubble sonoluminescence (SBSL) phenomenon. The remarkable finding here is that light is produced in very short pulses [9]: a million photons of several eV energy are emitted within 50 ps by apparently about 10^{10} atoms/molecules from a gas bubble of sub- μm radius.

The standard theoretical tool in the study of the bubble surface dynamics is the Rayleigh-Plesset (RP) equation, representing the motion of the gas-liquid interface by the time dependent (spherical) bubble radius $R(t)$. Several mechanisms which damp the collective motion of the bubble-liquid system have been incorporated in modern approaches: viscosity of the liquid and sound damping [4]. Effects of the ‘rectified’ mass diffusion [1, 5] and heat conductivity, see e.g. Ref. [10], play also an important role in establishing the parameter regime for stationary SBSL, but will not be further discussed here. In the SBSL cycle the sound emission produced during the violent bubble collapse turns out to be the most important energy loss mechanism [1, 11]. Less than half of the energy in the bubble is dissipated by the viscous friction. Only a comparatively tiny fraction of the energy delivered to the bubble by the external sound wave is radiated in form of the visible light [1, 11].

We will use the linear acoustic approximation (see Section 2.1), which describes the subsonic propagation of density perturbations in a fluid neglecting the effects of sound wave dispersion and absorption [2]. This approximation does not allow us to study situations involving shock wave formation in the liquid. In Section 2.2 we solve the sound wave equation for the velocity potential exactly for any given $R(t)$. Our derivation is formally exact provided the assumptions of non-dissipative fluid dynamics are valid. Our expressions account in full for retardation and allow an arbitrary incoming sound field. The key result is the exact form of the pressure amplitude radiated from the moving bubble surface into the surrounding liquid, see Eq. (28). In order to compare with earlier analytical and numerical work we also derive in Section 2.3 the perturbative expansion of our general results in powers of \dot{R}/c , i.e. bubble wall velocity divided by liquid sound velocity.

In the subsequent Section 3 we describe a model of the bubble interior which is motivated by the approximately homologous dynamics observed in numerical hydrodynamic simulations [12]: the gas density distribution and velocity field have been found to show a simple scaling behavior, in terms of the scaled radius variable $\xi \equiv r/R(t)$ and with $v(r, t) \approx \xi \dot{R}$, respectively. These numerical results have recently motivated development of a semianalytic approach for the coupled bubble-liquid system, based on a Lagrangian variational principle [13, 14], of which a simpler variant will be used here. This allows to assess the order of magnitude of the feedback effects of the bubble interior dynamics.

With this preparation we can proceed to the second step indicated above in Section 4, i.e. the derivation of a selfconsistent bubble equation of motion. There exists already a variety of equations generalizing the Rayleigh-Plesset equation, see e.g. [5, 6, 7], and more recent ones which consider the case of the externally driven damped nonlinear bubble oscillations in the SBSL parameter regime [3, 4]. In our selfconsistent approach (Section 4.1) we make extensive use of the results obtained in Section 2. We incorporate the external sound field in Section 4.2 according to standard experimental conditions realized to date. In Section 4.3 we derive a nonperturbative equation, Eq. (89), which is formally valid to all orders in \dot{R}/c (< 1), however, subject to the linear acoustic approximation scheme. We incorporate the bubble interior using the van der Waals equation of state and allow also for a realistic equation of state (EoS) of the liquid. Our derivations are based on the Navier-Stokes equation and, thus, take the effects of the liquid and gas viscosities consistently into account.

We illustrate our formal results in Section 5 by studying numerically the properties of an air bubble in water externally driven by an ultrasound field with system parameters in the typical SBSL regime [1, 11]. We show in detail there that the various (nonperturbative) corrections incorporated in the bubble equation of motion generally result in sizeable corrections of the maximal bubble surface velocity during the collapse. They tend to make the bubble collapse less violent than seen in previous perturbative descriptions. In Section 5.3 we compute the outgoing compression wave emitted from

the bubble surface into the surrounding liquid and consider the validity of the acoustic approximation. We present final remarks and conclusions accompanied by a brief summary of our work in Section 6.

2 Sound Emission from Phase Boundaries

We reexamine here the sound radiation originating from a moving phase boundary between two non-viscous fluids, separated by an idealized wall of vanishing thickness. References to earlier work on this subject are surveyed in Refs. [2, 6, 7]. Related issues were studied recently in Refs. [3, 4]. In distinction to these approaches, we derive exact expressions for the sound field emitted from a spherical boundary undergoing arbitrary motion. We begin in the next subsection by recapitulating some aspects of nonviscous hydrodynamics which lead to the (acoustic) approximation scheme used here in describing the sound generation and propagation.

2.1 Acoustic Approximation

The linear acoustic approximation is based on the assumption that the sound field causes only small perturbations of the ambient state of the fluid characterized by a vanishing velocity field and constant density and pressure Ref. [2]. Thus we shall not consider here nonlinear phenomena, such as the dispersion and absorption of sound waves in the medium and, in particular, the formation of supersonic shock waves. We shall see quantitatively in Section 5 that this scheme is fairly well satisfied, though the amplitude of the generated sound field typically reaches up to 10^4 atm near to a SBSL bubble.

The basic equations of nonviscous hydrodynamics are:

1. The continuity equation for the fluid density ρ , which assures the conservation of mass:

$$\partial_t \rho + \nabla \cdot (\rho \vec{v}) = 0 \quad , \quad (1)$$

where \vec{v} denotes the local fluid velocity.

2. The Euler equation, arising from Newton's equation of motion for a small fluid cell:

$$\rho D_t \vec{v} = -\nabla P \quad , \quad (2)$$

where P denotes the local pressure in the nonviscous fluid and the comoving derivative is defined by $D_t \equiv \partial_t + \vec{v} \cdot \nabla$. Later we will consider the Navier-Stokes generalization for viscous flow, see Eq. (53).

3. In the absence of entropy production the set of equations is closed by the EoS relating the pressure to the density. For example, the ideal gas EoS is:

$$P[\rho] = K \rho^\gamma \quad , \quad \gamma \equiv C_P/C_V \quad , \quad (3)$$

where the adiabatic index γ denotes the ratio of the specific heat at constant pressure and volume, respectively.

Had we allowed that the sound waves disturb the medium and generate entropy, we would require an EoS with two variables, e.g relating the pressure to the mass and energy densities. In this case we would have to introduce additionally the energy conservation in differential form, in order to close the set of equations.

In the following we study small-amplitude, acoustic perturbations of an ambient state of the fluid (liquid, gas) characterized by the ambient solutions to Eqs. (1)–(3), P_0 , \vec{v}_0 , ρ_0 . In order to obtain equations governing the perturbations P^* , \vec{v}^* , ρ^* , we set:

$$P = P_0 + P^* \quad , \quad \vec{v} = \vec{v}_0 + \vec{v}^* \quad , \quad \rho = \rho_0 + \rho^* \quad . \quad (4)$$

Inserting these expressions into Eqs. (1)–(3), a coupled set of equations results which relates various powers of the perturbations. The description of perturbations can be further simplified by assuming a particularly simple ambient state:

$$P_0(\vec{x}, t) = \text{Const.} , \quad \vec{v}_0(\vec{x}, t) = 0 , \quad \rho_0(\vec{x}, t) = \text{Const.} , \quad (5)$$

i.e. a homogeneous state independent of time (quiescent state). Then, the equations linearized in the perturbations become:

$$\partial_t \rho^* + \rho_0 \nabla \cdot \vec{v}^* = 0 , \quad (6)$$

$$\rho_0 \partial_t \vec{v}^* = -\nabla P^* , \quad (7)$$

$$P^* = \gamma K \rho_0^{\gamma-1} \rho^* = c^2 \rho^* , \quad c^2 \equiv \frac{\partial P}{\partial \rho} , \quad (8)$$

where we made use of a Taylor expansion in order to obtain Eq. (8) and introduced the (constant) sound velocity c for the ambient fluid state. Combining Eqs. (6)–(8), we obtain the well known wave equations:

$$\partial_t^2 P^* - c^2 \Delta P^* = 0 , \quad \partial_t^2 \rho^* - c^2 \Delta \rho^* = 0 . \quad (9)$$

Next, we introduce the velocity potential ϕ . Consider the curl of Eq. (7):

$$\rho_0 \partial_t \nabla \times \vec{v}^* = -\nabla \times \nabla P^* = 0 , \quad (10)$$

i.e. $\nabla \times \vec{v}^*(\vec{x}, t) = C(\vec{x})$. Thus, if the vorticity of the velocity field perturbation \vec{v}^* vanishes initially, then it remains zero always. In this case we can write:

$$\vec{v}^* \equiv \nabla \phi , \quad P^* \equiv -\rho_0 \partial_t \phi , \quad (11)$$

where the relation between the velocity potential and the pressure perturbation is chosen such that the linearized Euler equation, Eq. (7), is automatically satisfied. Inserting the EoS, Eq. (8), in the linearized continuity equation, Eq. (6), and using Eq. (11), one obtains the wave equation for the velocity potential:

$$\partial_t^2 \phi - c^2 \Delta \phi = 0 . \quad (12)$$

For simplicity, we suppress from now on the index $*$ introduced in Eq. (4).

2.2 Outgoing Spherical Wave Dynamics

Assuming spherical symmetry and using spherical coordinates, the velocity potential is seen to satisfy the usual scalar spherical wave equation:

$$0 = r \left\{ \partial_t^2 \phi - \frac{c^2}{r} \partial_r^2 (r\phi) \right\} = \partial_t^2 (r\phi) - c^2 \partial_r^2 (r\phi) . \quad (13)$$

The generic solutions (regular at infinity) are out- and ingoing spherical waves:

$$\phi_{out} = r^{-1} f(t - r/c) , \quad \phi_{in} = r^{-1} g(t + r/c) . \quad (14)$$

For the spherically symmetric bubble wall located at the position $r = R(t)$ the boundary condition is:

$$v(R, t) = \partial_r \phi(r, t)|_{r=R(t)} = \dot{R}(t) , \quad (15)$$

where we introduced the notation $\dot{X} \equiv dX/dt$. In general, the solution of the wave equation, Eq. (14), will be composed of a linear superposition of in- and outgoing spherical waves. We shall allow for the

possibility of an incoming acoustical wave, ϕ_{in} , e.g. as part of the external driving sound field, and rewrite Eq. (15) in more detail:

$$\partial_r \phi_{out}|_{r=R} = -\frac{1}{R^2} f(t - R/c) - \frac{1}{cR} f'(t - R/c) = \dot{R} - \partial_r \phi_{in}|_{r=R} \equiv \dot{\mathcal{R}} \quad , \quad (16)$$

where ϕ_{out} has been substituted by an outgoing spherical wave, cf. Eqs. (14); henceforth we use the abbreviation $f'(x) \equiv df/dx$. The external field ϕ_{in} is kept arbitrary in the derivations to follow, but will be incorporated according to a physically relevant example in Section 4.2.

In principle, there will be also a sound field generated by the moving phase boundary which will travel into the interior, to be reflected at the center of the bubble ($r = 0$), and then return. Its description, i.e. pertaining to the bubble interior, requires a suitable modification of the present approach, see Section 3.

With $\dot{\mathcal{R}}(t)$ given by other dynamics, our objective now is to determine implicitly the outgoing velocity potential ϕ_{out} . For this purpose we recast Eq. (16) into the form of an ordinary linear first-order differential equation with known time dependent coefficients:

$$-\frac{1}{R^2} F - \frac{1}{cR} \frac{1}{1 - \dot{R}/c} \dot{F} = \dot{\mathcal{R}} \quad , \quad (17)$$

where we used of the following substitutions and simple relations:

$$t_-(t) \equiv t - R(t)/c \implies \dot{t}_- = 1 - \dot{R}(t)/c \quad , \quad (18)$$

$$f'(t - R/c) = \frac{df}{dt_-} \frac{dt_-}{dt} \frac{1}{\dot{t}_-} = \frac{\dot{f}(t_-)}{1 - \dot{R}/c} \quad , \quad (19)$$

$$F(t) \equiv f(t_-(t)) \implies \dot{F}(t) = \dot{f}(t_-(t)) \quad . \quad (20)$$

In Eq. (17) we note the retardation factor originating in Eq. (19). The general solution of Eq. (17) is elementary:

$$\begin{aligned} F(t) &= F_0 \frac{R(t)}{R(t_0)} e^{-\int_{t_0}^t dt' \frac{c}{R(t')}} \\ &\quad - R(t) \int_{t_0}^t dt'' [c - \dot{R}(t'')] \dot{\mathcal{R}}(t'') e^{-\int_{t''}^t dt' \frac{c}{R(t')}} \quad , \end{aligned} \quad (21)$$

where $F_0 \equiv F(t_0)$ denotes the integration constant. It is fixed by the requirement that no outgoing wave should be excited before the bubble wall is set into motion at t_0 . Therefore, with $\dot{\mathcal{R}}(t < t_0) \equiv 0$, we find $F_0 = 0$. The resulting constraint $t > t_0$ is most conveniently implemented by a step function factor $\theta(t - t_0)$.

Using Eqs. (14), (20), we can recover from the above solution the outgoing velocity potential. To do this we will need the inverse function $\tilde{t}(t_-) \equiv t$ of $t_-(t)$, Eq. (18). Note that \tilde{t} is a single-valued function, if and only if $t_-(t) = t - R(t)/c$ is either strictly increasing or strictly decreasing with time. For subsonic bubble wall motion $t_-(t)$ is strictly increasing, since $1 - \dot{R}/c > 0$, and \tilde{t} is strictly increasing in this case. This allows us to perform variable substitution at will and we obtain:

$$\phi_{out}(r, t) = \frac{1}{r} F(\tilde{t}(t - r/c)) = -\theta(s - t_0) \frac{R(s)}{r} \int_{t_0}^s dt'' [c - \dot{R}(t'')] \dot{\mathcal{R}}(t'') e^{-\int_{t''}^s dt' \frac{c}{R(t')}} \quad , \quad (22)$$

$$s \equiv \tilde{t}(t - r/c) = t - \frac{r - R(s)}{c} \quad . \quad (23)$$

The retardation effect seen here can be evaluated more explicitly. For example:

$$\tilde{t}(t - r/c) \approx t - \frac{r - R(t - r/c)}{c}, \quad r \gg R(t), \quad (24)$$

$$\tilde{t}(t - r/c) \approx t - \frac{r - R(t)}{c}, \quad r \gtrsim R(t). \quad (25)$$

In order to calculate the velocity and pressure fields, we require the derivative of \tilde{t} :

$$\tilde{t}(t - R(t)/c) \equiv t \implies \tilde{t}'(t_-) = \frac{1}{1 - \dot{R}(\tilde{t}(t_-))/c}. \quad (26)$$

Then, differentiating Eq. (22), we obtain ($s > t_0$):

$$\begin{aligned} v(r, t) &= \partial_r[\phi_{out}(r, t) + \phi_{in}(r, t)] \\ &= \left\{ \frac{R\dot{R}}{r} + \left(\frac{1}{R} - \frac{1}{r}\right)\frac{F}{r} \right\}_{\tilde{t}(t-r/c)} + \partial_r\phi_{in}(r, t), \end{aligned} \quad (27)$$

$$\begin{aligned} P(r, t) &= -\rho_L \partial_t[\phi_{out}(r, t) + \phi_{in}(r, t)] \\ &= \frac{c\rho_L}{r} \left\{ R\dot{R} + \frac{F}{R} \right\}_{\tilde{t}(t-r/c)} - \rho_0 \partial_t\phi_{in}(r, t), \end{aligned} \quad (28)$$

where all functions within the braces are to be evaluated at the indicated time-argument $\tilde{t}(t - r/c) = s$; henceforth ρ_L denotes the ambient density of the liquid. We recall that P is the pressure perturbation due to the generated sound field, to be added to the ambient pressure.

2.3 Series Expansion for the Sound Field

The results obtained for the velocity potential and the velocity and pressure fields, Eqs. (21)–(28) in Section 2.2, involve an integration over the history of the bubble wall motion. Thus the corresponding nonlinear differential equation describing it selfconsistently (Section 4) could be expected to become nonlocal in time (see, however, Section 4.3). In any case, for sufficiently slow motion a local approximation can be justified, see Refs. [4, 5, 6, 7] and earlier references therein; this approach leads to a popular generalization of the RP equation. Therefore, our next objective is a systematic expansion in powers of \dot{R}/c of our general expressions, in particular of the velocity potential, Eq. (22).

Let us consider an integral of the form (in our case $j = c/R$, $/$, $h \propto (1 - \dot{R}/c)\dot{R}$):

$$I(s) \equiv \int_{t_0}^s dt'' h(t'') \exp\left\{-\int_{t''}^s dt' j(t')\right\}, \quad (29)$$

with $j > 0$ and $s \geq t_0$, cf. Eq. (21). For a sufficiently large integrand in the exponential the integration over t'' will be effectively limited to a small range next to the upper limit s . This suggests the following expansion:

$$\begin{aligned} I(s) &= \int_{t_0}^s dt'' h(t'') \exp\left\{-\int_{t''}^s dt' (j(t') - j(s))\right\} \exp\{j(s)(t'' - s)\} \\ &= \sum_{n=0}^{\infty} \frac{1}{n!} K^{(n)}(s) \frac{d^n}{dj^n} \int_{t_0}^s dt'' \exp\{j(s)(t'' - s)\} \\ &= \sum_{n=0}^{\infty} \frac{1}{n!} K^{(n)}(s) \frac{d^n}{dj^n} \frac{1 - \exp\{j(s)(t_0 - s)\}}{j(s)}, \end{aligned} \quad (30)$$

where:

$$K^{(n)}(s) \equiv \frac{d^n}{dt^n} h(\hat{t}) \exp\left\{-\int_{\hat{t}}^s dt' (j(t') - j(s))\right\} \Big|_{\hat{t}=s} . \quad (31)$$

We remark that the exponentially small correction term (for $s \gg t_0$) on the r.h.s. of Eq. (30) can be attributed to transient contributions to the integral or, rather, to the function F , Eq. (21), which are due to the switching-on of the bubble wall motion considered in Section 2.2. Since we will be mainly interested in the nonlinear oscillatory motion of the bubble wall when all transients have died out, we can neglect this term for sufficiently late times. Thus, we obtain:

$$I(s) = \sum_{n=0}^{\infty} (-1)^n K^{(n)}(s) j^{-n-1}(s) , \quad (32)$$

which presents the starting point of our approximate evaluation of the velocity potential.

Employing Eqs. (21), (22) from the previous section together with Eqs. (29), (32) above, we obtain:

$$\begin{aligned} \phi_{out}(r, t) = & \quad (33) \\ & -\frac{R^2(s)}{r} \sum_{n=0}^{\infty} \left(-\frac{R(s)}{c}\right)^n \frac{d^n}{dt^n} \left(1 - \frac{\dot{R}(\hat{t})}{c}\right) \dot{\mathcal{R}}(\hat{t}) \exp\left\{(s - \hat{t}) \frac{c}{R(s)} + \int_s^{\hat{t}} dt \frac{c}{R(t)}\right\} \Big|_{\hat{t}=s} \\ = & -\frac{R^2}{r} \dot{\mathcal{R}} \left\{ 1 - 2\frac{\dot{R}}{c} \left(1 + \frac{1}{2} \frac{R\ddot{\mathcal{R}}}{\dot{R}\dot{\mathcal{R}}}\right) + 2\left(\frac{\dot{R}}{c}\right)^2 \left(1 + 2\frac{R\ddot{\mathcal{R}}}{\dot{R}\dot{\mathcal{R}}} + \frac{R\ddot{R}}{\dot{R}^2} + \frac{1}{2} \frac{R^2 \ddot{\mathcal{R}}}{\dot{R}^2 \dot{\mathcal{R}}}\right) + \mathcal{O}\left((\dot{R}/c)^3\right) \right\}_s , \end{aligned}$$

where as before $s = \tilde{t}(t - r/c)$ see Eq. (23). The expansion has to be carried out up to order $n = 4$ in order to acquire in the \dot{R}/c expansion all second order terms. Our result reduces to Eq. (18) of Ref. [4] at the $\mathcal{O}(\dot{R}/c)$ obtained there, provided we replace i) $\mathcal{R}(t) \rightarrow R(t)$, i.e. we ignore effects of an incoming sound field, cf. Eq. (16), and ii) $\tilde{t}(t - r/c) \rightarrow t - [r - R(t)]/c$. The latter approximation amounts to neglecting already some $\mathcal{O}(\dot{R}/c)$ corrections in Eq. (33) due to retardation effects.

To conclude this subsection, we calculate the velocity and pressure fields generated by a driven oscillating bubble wall, i.e. the sound emitted, by combining Eqs. (22), (27) and (28), respectively, and Eq. (33):

$$\begin{aligned} v(r, t) = & \partial_r \phi_{in}(r, t) + \frac{R^2 \dot{\mathcal{R}}}{r^2} \\ & + 2\frac{\dot{R}}{c} \frac{R\dot{\mathcal{R}}}{r} \left(1 - \frac{R}{r}\right) \left\{ 1 + \frac{1}{2} \frac{R\ddot{\mathcal{R}}}{\dot{R}\dot{\mathcal{R}}} - \frac{\dot{R}}{c} \left(1 + 2\frac{R\ddot{\mathcal{R}}}{\dot{R}\dot{\mathcal{R}}} + \frac{R\ddot{R}}{\dot{R}^2} + \frac{1}{2} \frac{R^2 \ddot{\mathcal{R}}}{\dot{R}^2 \dot{\mathcal{R}}}\right) + \mathcal{O}\left((\dot{R}/c)^2\right) \right\}_{\tilde{t}(t-r/c)} , \end{aligned} \quad (34)$$

which illustrates nicely that our expansion reproduces the incompressible fluid ($c \rightarrow \infty$) limit; furthermore:

$$\begin{aligned} P(r, t) = & -\rho_L \partial_t \phi_{in}(r, t) \\ & + \frac{2\rho_L}{r} R\dot{\mathcal{R}} \left\{ 1 + \frac{1}{2} \frac{R\ddot{\mathcal{R}}}{\dot{R}\dot{\mathcal{R}}} - \frac{\dot{R}}{c} \left(1 + 2\frac{R\ddot{\mathcal{R}}}{\dot{R}\dot{\mathcal{R}}} + \frac{R\ddot{R}}{\dot{R}^2} + \frac{1}{2} \frac{R^2 \ddot{\mathcal{R}}}{\dot{R}^2 \dot{\mathcal{R}}}\right) + \mathcal{O}\left((\dot{R}/c)^2\right) \right\}_{\tilde{t}(t-r/c)} , \end{aligned} \quad (35)$$

where the inverse of the retarded time function has to be inserted everywhere as indicated before.

3 Homologous Bubble Interior Dynamics

In section 4 we want to derive the equation of motion of the phase boundary (bubble surface) self-consistently. For this purpose we need to understand the dynamics of the interior of the bubble. In distinction to Section 2, presently we have to take into account that the density, pressure, and velocity fields inside the bubble may change by several orders of magnitude during different phases of the (periodic) bubble motion. Therefore, a linearization of the hydrodynamic equations of motion around a homogeneous and time independent ambient state, as performed in Section 2.1, is not applicable here.

In the hydrodynamic studies of the interior motion the emphasis has been to understand the development of the extreme conditions inside the bubble [15, 16]. Chu noted that for an important part of the SBSL cycle the bubble motion is (nearly) homologous, i.e. the shape of the density distribution and the velocity field of the gas scale in an appropriate way with the radius R and surface velocity \dot{R} [12]. The numerical simulations in the SBSL parameter regime indicate a homologous contraction (and its stability) until the onset of shock wave formation and independently of the details of the EoS used. This stability of the homologous motion may be related to the fact that only for the homologous motion there is no energy loss due to viscosity inside the bubble (see Eq. (60) and below).

We solve the continuity and Euler equations, Eqs. (1) and (2) of Section 2.1 respectively, by approximating the density and velocity fields with suitable scaling functions. We neglect dissipative effects in the bubble, such as viscosity, heat conduction, and radiation transfer especially. Presently, we are interested in a semiquantitative analysis of the bubble interior. This seems sufficient for our later derivation of the overall bubble dynamics: the motion is largely determined by the dynamics of the fluid, since only a minor fraction of the relevant total energy resides in the interior at any time. For a detailed understanding of the microscopic processes leading to sonoluminescence inside the bubble, however, the dissipative effects will be essential ingredients.

It turns out, see Refs. [13, 14], that for a time independent shape of a properly scaling density distribution the velocity potential is:

$$\phi(r, t) \equiv \frac{1}{2} \frac{\dot{R}}{R} r^2, \quad r \leq R, \quad (36)$$

in terms of the bubble radius $R(t)$, which yields:

$$v = \partial_r \phi = \frac{\dot{R}}{R} r, \quad \partial_t \phi = \frac{1}{2} \left(\frac{\ddot{R}}{R} - \left(\frac{\dot{R}}{R} \right)^2 \right) r^2, \quad (37)$$

i.e. a linear radial velocity profile. The continuity equation, Eq. (1), takes the form:

$$0 = \partial_t \rho + \frac{1}{r^2} \partial_r (r^2 \rho v) = \left(\dot{\varrho} + 3 \frac{\dot{R}}{R} \varrho \right) \tilde{d} + \varrho \partial_t \tilde{d} \Big|_{\xi}, \quad (38)$$

where we introduced the homologous ansatz:

$$\rho(r, t) \equiv \varrho(t) \tilde{d}(\xi, t), \quad (39)$$

with $\xi \equiv r/R(t)$ denoting the scaling variable. Here we find indeed that the velocity potential, Eq. (36), is consistent with a time independent density profile function, i.e.

$$\tilde{d}(\xi, t) = d(\xi), \quad (40)$$

and the overall density factor of Eq. (39), normalized to N particles inside the bubble:

$$\varrho(t) = \frac{N}{4\pi R^3(t) \int_0^1 d\xi \xi^2 d(\xi)}. \quad (41)$$

We choose $d(1) \equiv 1$ in the following, i.e. $\rho(R, t) = \varrho(t)$. We refer the reader to Refs. [13, 14] for the variational improvement of the strictly homologous dynamics (see [12] and references therein) which we will pursue here, with a time independent yet scaling density profile function.

In order to determine the scaling function $d(\xi)$, we consider the integral of the Euler equation, cf. Eq. (2), which for our radially symmetric case yields:

$$\partial_t \phi|_R^r + \frac{1}{2}(\partial_r \phi)^2|_R^r = - \int_R^r dr \frac{1}{\rho} \partial_r P . \quad (42)$$

In the absence of entropy S production the integral on the r.h.s. is the enthalpy:

$$\int_r^R dr \frac{1}{\rho} \partial_r P = \int_r^R \frac{dP}{\rho}|_S = h(R) - h(r), \quad h = \mathcal{E} + \frac{P}{\rho} , \quad (43)$$

where $\mathcal{E} = E/N$ is the specific energy per particle.

During the highest compression particle densities reached in the bubble interior are similar to those in the liquid outside. We thus use here for the gas an adiabatic EOS, cf. Eq. (3), with van der Waals hard core corrections:

$$P(\rho) = P_0 \left(\frac{\rho}{\rho_0} \right)^\gamma \left(\frac{\rho_a - \rho_0}{\rho_a - \rho} \right)^\gamma \equiv \tilde{P}_0 \left(\frac{\rho/\rho_0}{1 - \rho/\rho_a} \right)^\gamma . \quad (44)$$

Here $\rho_0 (\ll \rho_a)$ is the density at which the bubble interior is at the ambient pressure P_0 and $\rho_a^{-1} \equiv \frac{4\pi}{3} a^3 / N$ in terms of the van der Waals excluded volume. The adiabatic index γ for ideal monatomic (diatomic) gases is 5/3 (7/5). Related EoS have been applied to calculate the gas pressure before [4, 13, 15].

Performing the integral in Eq. (42) using Eq. (44) and employing the scaling form for the velocity potential, Eq. (36), we obtain ($\xi \equiv r/R(t)$):

$$\frac{1}{2} R \ddot{R} (\xi^2 - 1) = - \frac{\tilde{P}_0}{\rho_0} \left(\frac{\rho/\rho_0}{1 - \rho/\rho_a} \right)^{\gamma-1} \left(\frac{1}{1 - \rho/\rho_a} + \frac{1}{\gamma - 1} \right) \Big|_R^r , \quad (45)$$

$$= - \frac{\tilde{P}_0}{\rho_0} \left(\frac{\rho}{\rho_0} \right)^{\gamma-1} \left(\frac{\gamma}{\gamma - 1} + \mathcal{O}(\rho/\rho_a) \right) \Big|_R^r , \quad (46)$$

$$= - \frac{\tilde{P}_0}{\rho_a} \left(\frac{\rho_a}{\rho_0} \right)^\gamma \frac{1}{(1 - \rho/\rho_a)^\gamma} (1 + \mathcal{O}(1 - \rho/\rho_a)) \Big|_R^r , \quad (47)$$

where Eq. (46) and Eq. (47), respectively, represent the low- and high-density limits of the r.h.s. of Eq. (45).

Obviously, the van der Waals correction introduces an additional scale which makes it difficult to find a universal density shape function. Therefore, we consider the low- and high-density cases in turn:

- **Low density.** Inserting Eqs. (39)–(41) into Eq. (46), we obtain:

$$\frac{\gamma - 1}{2\gamma} \frac{\rho_0 R \ddot{R}}{\tilde{P}_0} \left(\frac{\rho_0}{\varrho(t)} \right)^{\gamma-1} = q_1 = \frac{d^{\gamma-1}(\xi) - 1}{1 - \xi^2} . \quad (48)$$

Since the l.h.s. here only depends on t and the r.h.s. only on ξ , we have introduced a constant parameter q_1 characterizing the time independent density profile. Solving the r.h.s., we find:

$$d_1(\xi) = \left(1 + q_1(1 - \xi^2) \right)^{\frac{1}{\gamma-1}} . \quad (49)$$

We note that the l.h.s. of Eq. (48) determines the value of the parameter q_l , and thus we can verify if indeed it is time independent. From this we conclude that this low-density ($\rho \ll \rho_a$) functional form of the density profile function is approximately valid for inertial motion with $\ddot{R} \approx 0$ or, more generally, when the bubble wall accelerates (decelerates) proportional to the internal pressure acting on it, $P(R, t) \approx \tilde{P}_0(\varrho(t)/\rho_0)^\gamma$, that is whenever the ratio $\{\varrho R \ddot{R}\}(t)/P(R, t)$ is approximately constant.

- **High density.** In this limit, inserting Eqs. (39)–(41) into Eq. (47), we obtain:

$$\frac{1}{2\gamma} \left(\frac{\rho_0}{\rho_a} \right)^\gamma \frac{\rho_a R \ddot{R}}{\tilde{P}_0} \frac{(1 - \varrho(t)/\rho_a)^{\gamma+1}}{\varrho(t)/\rho_a} = q_h = \frac{d(\xi) - 1}{1 - \xi^2} , \quad (50)$$

where again the l.h.s. is only a function of time, while the r.h.s. is only a function of ξ , and thus we can introduce the constant q_h . In deriving Eq. (50), we employed an additional expansion for $d(\xi) \approx 1$ on the r.h.s. which is consistent with the high-density case ($\rho \approx \rho_a$) under consideration. Solving the r.h.s. for the density profile function, we obtain:

$$d_h(\xi) = 1 + q_h(1 - \xi^2) , \quad (51)$$

while the l.h.s. determines the value of the parameter q_h , as before. The limit of validity of this result is controlled by the requirement that the expression on the l.h.s. remains time independent. Note that the high- and low-density profiles agree with each other for $\gamma = 2$; however, $\gamma = 3/2$ and $5/2$ for mono- and diatomic gases, respectively.

We remark that the numerical values of q_l and q_h , in general, vary depending on the dynamical regime, and always $q \geq -1$. It is important to realize that Eqs. (48) and (50) present implicit equations for q_l and q_h , respectively. The reason for this is that $\varrho(t)$ because of the normalization in Eq. (41) depends on the integrated density profile and thus on the respective q by Eqs. (49), (51). In practice, these ‘constants’ will be treated as adiabatically changing parameters to be computed selfconsistently from the equations derived here.

We observe that as the bubble goes through the cycle determined by the driving pressure, the shape of the matter distribution inside the bubble changes, controlled by q , which remains nearly constant during much of the cycle and changes rapidly in sign near to the bubble collapse/bounce, whenever $\ddot{R} = 0$, where the l.h.s. of Eqs. (45), (48), or (50) vanishes, and $q = 0$, assuring in this transition instant a (nearly) homogeneous density distribution. For negative values of q the highest density is found at the surface, corresponding to a collapsing phase; similarly, positive values of q with the highest density at the center correspond to an expanding phase of the bubble motion. We found that there is an approximate fixed point $r/R \equiv \xi_*$ in the motion, where the average density corresponding to a homogeneous bubble is maintained during the entire cycle:

$$\rho_* \equiv \rho(\xi_* R, t) \simeq N/(4\pi/3 R(t)^3) , \quad \xi_* \approx 0.78 . \quad (52)$$

This will turn out to be a very useful property which we shall exploit deriving specific numerical results in Section 5.2, where we compare the bubble dynamics for a homogeneous and a homologous interior, respectively.

4 Derivation of the Bubble Equation of Motion

Having studied the effects of a given bubble wall motion on the exterior liquid and the bubble interior in Sections 2 and 3, respectively, we now turn to the question how this motion can be determined selfconsistently. That is, assuming an external driving sound field ϕ_{in} , we want to derive an equation of

motion for the bubble radius R as a function of time. We also take the bubble interior into account. Its dynamics may have little influence on most of the cycle of stable bubble oscillations. However, in order to improve the understanding of the final stage of the violent collapse [13, 14], it has to be considered. Besides the sound emission from the moving phase boundary, which constitutes a major energy loss mechanism, the effect of viscous damping will also be incorporated here, which is of a similar order of magnitude as acoustic damping. Despite the fact that our considerations so far were based on the assumption of nonviscous fluid dynamics, i.e. approximately free wave propagation in particular, we can include dissipative and driving forces into the equation of motion for $R(t)$ by deriving it from the Navier-Stokes (momentum balance) equation. Thus, only the backreaction of viscosity (and other dissipative transport effects) on the wave propagation and velocity potential ϕ is neglected here.

4.1 The (Generalized) Rayleigh-Plesset Equation

We begin with the Navier-Stokes equation generalizing the Euler equation, see Eq. (2), to the case of viscous fluids [2]. For our spherically symmetric situation this equation can be written in the form:

$$\partial_r \left\{ \partial_t \phi + \frac{1}{2} (\partial_r \phi)^2 \right\} = -\frac{1}{\rho} \partial_r P + \frac{\eta}{\rho} \partial_r \left(\frac{1}{r} \partial_r^2 (r\phi) \right) , \quad (53)$$

where $\phi(r, t)$ denotes the appropriate velocity potential, i.e. for the interior or exterior region, and $\eta \equiv \frac{4}{3}\eta_s + \eta_b$ is the relevant combination of shear and bulk viscosities of the fluid entering here. Similarly, the pressure P has to be specified differently according to whether the interior or exterior of the bubble is considered.

Due to the phase change at the bubble surface, there arises a nontrivial boundary condition relating the normal components of the stress tensor Σ inside (*Gas*) and outside (*Liquid*):

$$\vec{n} \cdot \Sigma_G \cdot \vec{n} = \vec{n} \cdot \Sigma_L \cdot \vec{n} - \frac{2\sigma}{R} , \quad (54)$$

where the term $\propto \sigma$ denotes the ‘pressure’ contribution due to the (liquid) surface tension for the liquid/gas interface and the viscous stress tensor has to be evaluated for the respective fluid under consideration [2]:

$$\vec{n} \cdot \Sigma \cdot \vec{n} \equiv \left\{ -P + \eta \partial_r v - \frac{\bar{\eta}}{r} v \right\}_{r=R} , \quad (55)$$

where $\bar{\eta} \equiv \frac{4}{3}\eta_s - 2\eta_b$, η was defined after Eq. (53), and $v(r, t) \equiv \partial_r \phi(r, t)$, as usual. Then, employing the boundary condition (15) and the velocity potential (36) for the gas phase, we obtain instead of Eq. (54) more explicitly:

$$-P_G(R) + (\eta_G - \bar{\eta}_G) \frac{\dot{R}}{R} = -P_L(R) + \eta_L \partial_r v|_{r=R} - \bar{\eta}_L \frac{\dot{R}}{R} - \frac{2\sigma}{R} . \quad (56)$$

Using Eq. (26) and the velocity field (34), we calculate $\partial_r v|_R$ for the outer liquid:

$$\begin{aligned} \partial_r v(r, t)|_{r=R} &= -2 \frac{\dot{R}}{R} - \dot{R}^{-1} \left\{ \left[-2 \frac{\dot{R}}{R} + \frac{\dot{R}}{c} \partial_t + \left(\frac{\dot{R}}{c} \right)^2 \partial_t^2 \right] \partial_r \phi_{in}(r, t) \right\}_{r=R} \\ &\quad - 2 \frac{\dot{\mathcal{R}}}{R} \left(\frac{\dot{R}}{c} \right)^2 \left(1 + 2 \frac{R\ddot{\mathcal{R}}}{\dot{R}\dot{\mathcal{R}}} + \frac{R\ddot{R}}{\dot{R}^2} + \frac{1}{2} \frac{R^2 \ddot{\mathcal{R}}}{\dot{R}^2 \dot{\mathcal{R}}} \right) + \mathcal{O} \left((\dot{R}/c)^3 \right) , \end{aligned} \quad (57)$$

where the first term on the RHS corresponds to the incompressible fluid limit ($c \rightarrow \infty$) in the absence of an external driving sound field.

Several remarks are in order here:

- The bubble gas pressure at the surface, $P_G(R) \equiv P_G(\rho_G(R, t))$, is determined by the van der Waals EoS Eq. (44) together with $\rho_G(R, t) = \varrho_G(t)$, according to Eqs. (39), (41) for the homologous density function. The liquid vapor pressure inside the bubble is not considered at present.
- We observe that $\eta_G - \bar{\eta}_G = 3\eta_{bG}$, in terms of the bulk viscosity of the gas, which is generally very small compared to liquid viscosities. The shear viscosity does not contribute here at all, cf. also the remark after Eq. (60) below. For completeness, we allow for viscous damping in the gas inside the bubble, even though it might at best become important during the rapid collapse and high compression phase.
- We recall that by definition of the inverse of the retarded time function, Eq. (26), we have $\tilde{t}(t - R(t)/c) \equiv t$; therefore, the r.h.s. of Eq. (57) has to be evaluated at the time t .

In the following the boundary condition (56) together with Eq. (57) will be employed to eliminate $P_L(R)$ in terms of the other quantities which by now are explicitly calculated functions of R , \dot{R} , \ddot{R} etc. In order to proceed, we convert the Navier-Stokes equation (53) together with the boundary condition (56) into an ordinary differential equation for $R(t)$. This can be achieved by integrating over the radial coordinate, i.e. the approach advocated earlier in Ref. [3], for example. Symbolically, in obvious correspondence with the terms on the left- and right-hand sides of Eq. (53), we obtain:

$$\left\{ \int_0^R + \int_R^\infty \right\} dr \mathcal{D} = \left\{ \int_0^R + \int_R^\infty \right\} dr \mathcal{P} + \left\{ \int_0^R + \int_R^\infty \right\} dr \mathcal{V} , \quad (58)$$

where we split the integrations at $r = R$ because of the different phases inside and outside. Making use of the results of the previous Sections 2 and 3, we proceed to evaluate each term of the generalized Bernoulli equation (58) in turn.

Using the velocity potential (36) for the bubble interior, we obtain:

$$\int_0^R dr \mathcal{D} \equiv \int_0^R dr \partial_r \left\{ \partial_t \phi + \frac{1}{2} (\partial_r \phi)^2 \right\} = \frac{1}{2} R \ddot{R} , \quad (59)$$

$$\int_0^R dr \mathcal{V} \equiv \int_0^R dr \frac{\eta_G}{\rho} \partial_r \left(\frac{1}{r} \partial_r^2 (r \phi) \right) = 0 . \quad (60)$$

We observe that the homologous scaling solution for the bubble interior, $\phi \propto r^2$, does not give a contribution to the integrated viscous force term here. This remarkable result suggests that viscous forces drive the bubble motion to the homologous limit which we discussed in Section 3 and which is in this respect quite unique [12, 13, 14].

Furthermore, employing the van der Waals EoS (44), we calculated the enthalpy integral for the gas inside the bubble before, cf. Eqs. (43), (45):

$$\int_0^R dr \mathcal{P} \equiv - \int_0^R dr \frac{1}{\rho} \partial_r P_G = - P_G(\rho_G) \frac{\gamma - \rho_G/\rho_a}{(\gamma - 1)\rho_G} \Big|_0^R \equiv h_G[P_G] , \quad (61)$$

where we rewrote our previous result of Eq. (45) in terms of the van der Waals expression for the pressure and denote by h_G the gas enthalpy.

Next, we turn to the evaluation of the corresponding integrals for the exterior region. The first integral follows immediately from our derivations in Section 2:

$$\int_R^\infty dr \mathcal{D} \equiv \int_R^\infty dr \partial_r \left\{ \partial_t \phi + \frac{1}{2} (\partial_r \phi)^2 \right\} = \frac{1}{\rho_L} P(R, t) - \frac{1}{2} \dot{R}^2 , \quad (62)$$

where $P(r, t)$ denotes the pressure field calculated in Eq. (28) and evaluated approximately in Eq. (35); henceforth we denote by ρ_L the ambient density of the liquid. The second term on the r.h.s. of

Eq. (62) simply follows from the boundary condition (15) and the assumption $\phi \rightarrow 0$ (sufficiently fast) for $r \rightarrow \infty$.

In order to calculate the enthalpy integral for the liquid, we employ an EoS which gives a realistic description for many liquids [5]:

$$P_L(\rho) = (P_0 + P_1) \left(\frac{\rho}{\rho_L} \right)^n - P_1, \quad \frac{\partial P_L}{\partial \rho} = c^2(\rho), \quad (63)$$

where P_0 denotes the ambient pressure and n, P_1 are parameters depending on the liquid (e.g. for water $n = 7, P_1 = 3 \text{ kbar}$). Then, it is straightforward to obtain:

$$\int_R^\infty dr \mathcal{P} \equiv - \int_R^\infty dr \frac{1}{\rho} \partial_r P_L = \frac{n}{n-1} \frac{P_0 + P_1}{\rho_L} \left\{ \left(\frac{P_L(R) + P_1}{P_0 + P_1} \right)^{\frac{n-1}{n}} - 1 \right\} \equiv h_L[P_L], \quad (64)$$

using $P(r \rightarrow \infty) = P_0$, i.e. the ambient pressure, and where h_L denotes the liquid enthalpy. As mentioned before, the liquid pressure on the bubble surface, $P_L(R)$, will be eliminated via the pressure boundary condition (56).

The last (viscous) term from Eq. (58) can be evaluated employing the approximation $\rho \approx \rho_L$:

$$\int_R^\infty dr \mathcal{V} \equiv \int_R^\infty dr \frac{\eta_L}{\rho} \partial_r \left(\frac{1}{r} \partial_r^2(r\phi) \right) = -\frac{\eta_L}{\rho_L} \frac{1}{r} \partial_r^2(r\phi)|_{r=R} = -\frac{\eta_L}{\rho_L} \left\{ 2 \frac{\dot{R}}{R} + \partial_r v|_{r=R} \right\}, \quad (65)$$

i.e. neglecting a cross term between viscosity and compressibility of the liquid, which will be justified by the numerical results presented in Section 5.3.

It is worth while to recall that in Eqs. (59)–(65) all the functions R, \dot{R}, \ddot{R} , etc., which appear on the r.h.s., are to be evaluated simply at the time t .

Collecting the essential results from Eqs. (59)–(65), we obtain the equation of motion for the bubble radius $R(t)$, i.e. $\int_0^\infty dr \mathcal{D} = \int_0^\infty dr (\mathcal{P} + \mathcal{V})$, in the form:

$$\frac{1}{2} R \ddot{R} - \frac{1}{2} \dot{R}^2 + \frac{1}{\rho_L} P(R, t) = h_G[P_G] + h_L[P_L] - \frac{\eta_L}{\rho_L} \left\{ 2 \frac{\dot{R}}{R} + \partial_r v|_{r=R} \right\}. \quad (66)$$

This equation is valid for any subsonic bubble wall velocity, it is nonperturbative in \dot{R}/c . In fact, inserting here our general results of Section 2.2 for the sound field generated by the bubble, in particular $v(r, t)$ and $P(r, t)$ calculated in Eqs. (27) and (28) respectively, we obtain an important generalization of the Rayleigh-Plesset equation.

In order to illustrate the contents of Eq. (66), we proceed with a perturbative evaluation of terms involving the generated sound field making use of our results of Section 2.3. Using in Eq. (66) the expansions in \dot{R}/c , especially Eqs. (35), (57), we obtain the perturbative bubble equation of motion:

$$\begin{aligned} & \frac{1}{2} R \ddot{R} - \frac{1}{2} \dot{R}^2 + \frac{1}{\rho_L} P_a + 2 \dot{R} \dot{\mathcal{R}} \left(1 - \frac{\dot{R}}{c} \right) + R \ddot{\mathcal{R}} \left(1 - 4 \frac{\dot{R}}{c} \right) - \frac{2}{c} R \dot{\mathcal{R}} \ddot{R} - \frac{1}{c} R^2 \ddot{\mathcal{R}} \\ &= h_G[P_G] + h_L[P_L] - 2 \frac{\eta_L}{\rho_L} \left\{ \left[\frac{1}{R} - \frac{1}{2c} \partial_t \right] v_a(r, t) \right\}_{r=R} + \mathcal{O}((\dot{R}/c)^2). \end{aligned} \quad (67)$$

We observe that for $\dot{\mathcal{R}} \equiv 0$, i.e. when the bubble wall velocity is identical to the incoming acoustical velocity field at $r = R(t)$, all terms involving $1/c$ -corrections vanish. However, on the r.h.s. the viscous damping term survives, which involves only the incoming sound field. This is to be expected, since no outgoing sound wave is generated, in agreement with the nonperturbative results for the velocity and pressure fields, $v = v_a \equiv \partial_r \phi_{in}$ and $P = P_a \equiv -\rho_L \partial_t \phi_{in}$ in this case.

We arrive at a more useful form of the bubble equation of motion by eliminating \ddot{R} from Eq. (67). This can be achieved at the same order in \dot{R}/c by using the equation at leading order (i.e. for $c \rightarrow \infty$) to calculate \ddot{R} and then \ddot{R} :

$$R \ddot{R} = \frac{2}{3} \left\{ \frac{d}{dt} [\text{r.h.s.}|_{\infty}] - \frac{9}{2} \dot{R} \ddot{R} - \frac{1}{\rho_L} \dot{P}_a + 2 \ddot{R} v_a + 3 \dot{R} \dot{v}_a + R \ddot{v}_a \right\} , \quad (68)$$

where the term $[\text{r.h.s.}|_{\infty}]$ denotes the r.h.s. of Eq. (67) in the limit $c \rightarrow \infty$ and $P_a \equiv P_a(R, t)$, $v_a \equiv v_a(R, t)$, $\dot{P}_a \equiv \frac{d}{dt} P_a(R, t)$, $\dot{v}_a \equiv \frac{d}{dt} v_a(R, t)$, etc., from now on. Reinserting this expression into Eq. (67), we finally obtain the equation:

$$\begin{aligned} & R \ddot{R} \left(\left(1 + \frac{1}{2}\right) \left(1 - 2 \frac{\dot{R}}{c}\right) + \frac{2}{3} \frac{v_a}{c} \right) + \frac{3}{2} \dot{R}^2 \left(1 - \frac{4}{3} \frac{\dot{R} - v_a}{c}\right) \\ & - 2 \dot{R} v_a - R \dot{v}_a \left(1 - (1 + \underline{1}) \frac{\dot{R}}{c}\right) + \frac{1}{3} \frac{R^2}{c} \ddot{v}_a \\ & - \left[1 + \left(1 - \frac{1}{3}\right) \frac{R}{c} \frac{d}{dt} \Big|_{c \rightarrow \infty} \right] \left[h_G[P_G] + h_L[P_L] - 2 \frac{\eta_L}{\rho_L} \left\{ \left[\frac{1}{R} - \frac{1}{2c} \partial_t \right] v_a(r, t) \right\}_{r=R} - \frac{1}{\rho_L} P_a \right] \\ & + O\left((\dot{R}/c)^2\right) = 0 , \end{aligned} \quad (69)$$

where we separated out the underlined terms, in order to facilitate the discussion of our result; the term $\propto d/dt|_{c \rightarrow \infty}$ is to be read as: take this limit of the following expression before evaluating the derivative. Equation (69) generalizes previously considered variants of the Rayleigh-Plesset equation. In comparison to earlier related work, particularly Refs. [3, 4, 13], we draw attention to the following:

- The dynamics of the gas in the interior of the bubble as well as of the exterior liquid is fully incorporated in our derivation. It is based on the Navier-Stokes equation (53) supplemented by the boundary condition (56) relating the normal components of the stress tensor at the bubble surface. Neglecting the bubble interior amounts to setting the underlined numerical constants in Eq. (69) to zero, equivalent to neglecting $R\ddot{R}/2$ in Eq. (66), and setting $h_G[P_G] \equiv 0$ in both equations. These apparently are sizeable corrections which were not considered previously. However, these terms cancel exactly, if the homologous dynamics of Section 3 is applicable for the bubble interior. Also, according to Eq. (61), $h_G = 0$ for a homogeneous bubble.
- The influence of the external acoustic driving field is consistently taken into account in our treatment of the sound field outside of the bubble. The terms $\propto v_a$, i.e. the incoming velocity field, or its derivatives, were neglected before; only terms involving the driving pressure P_a had been obtained. These additional terms are necessary to restore the boundary condition on the sound field at $r = R(t)$, see the comment after Eq. (67).
- A realistic EoS for the liquid, Eq. (63), has been employed here. For $n \gg 1$ the enthalpy $h_L[P_L]$ in Eqs. (66), (69) reduces to $(P_L(R) - P_0)/\rho_L$, which was used earlier instead. – The viscous term $\propto \eta_L$ was not studied before.
- The pressure boundary condition (56) contains terms which have been neglected before:

$$\begin{aligned} P_L(R) &= P_G(R) - \frac{2\sigma}{R} - (3\eta_{bG} + 4\eta_{sL}) \frac{\dot{R}}{R} \\ &+ \left(\frac{4}{3}\eta_{sL} + \eta_{bL}\right) \left(\frac{2}{R} v_a - \frac{1}{c} \{\partial_t v_a(r, t)\}_R\right) + O\left((\dot{R}/c)^2\right) , \end{aligned} \quad (70)$$

where we used Eq. (57) and inserted the shear and bulk viscosities for liquid and gas explicitly. Except for a highly compressed or, rather, very hot gas [2], its bulk viscosity presents a negligible contribution in Eq. (70), being on the %-level as compared to liquid water at most. However, we also note the corrections due to the incoming sound field.

If we discard altogether the modifications just discussed, we reproduce Eqs. (9) and (10) of Ref. [4]. In Section 5 we will explore numerically the effects of the corrections presently discussed.

4.2 The Driving Sound Field

Having further studies of single bubble sonoluminescence in mind, we determine here those quantities entering our results which depend on the external acoustic driving field. For typical experiments on single bubble sonoluminescence carried out to date the driving sound frequency is approximately $\nu \approx 25$ KHz, which translates into a wavelength of $\lambda \approx 5.9$ cm given the sound velocity in water of $c = 1481$ m/s. Relevant bubble radii are such that $R/\lambda \lesssim 10^{-3}$ [4, 17]. Therefore, we consider the external field in the long-wavelength limit.

Following Ref. [4], we assume a plane standing wave: $\phi = A \sin(kz) \cos(\omega t)$, i.e. along the z -axis with $\omega \equiv 2\pi\nu$ and $k \equiv 2\pi/\lambda = \omega/c$. In the long-wavelength limit, with $r \lesssim R \ll 1/k$, the spherical component of the external field, ϕ_{in} , determines the dominant driving force for spherically symmetric bubble oscillations. Expressing $z = z_0 + r \cos \theta$, where z_0 denotes the presently irrelevant position of the center of the bubble, we can project out the spherically symmetric monopole component of the driving field to obtain:

$$\phi_{in}(r, t) = \frac{A}{2} \cos(\omega t) \int_{-1}^1 d(\cos \theta) P_0(\cos \theta) \sin(k[z_0 + r \cos \theta]) = A \sin(kz_0) \cos(\omega t) \frac{\sin(kr)}{kr} , \quad (71)$$

with $P_0 \equiv 1$ denoting the appropriate Legendre polynomial.

We recall that $P(R, t)$ contains the contribution of the incoming sound field, i.e. the external “acoustic driving pressure”:

$$\begin{aligned} P_a(r, t) &\equiv -\rho_L \partial_t \phi_{in}(r, t) \\ &= P_A \sin(\omega t) \frac{\sin(kr)}{kr} = P_A \sin(\omega t) \left(1 - \frac{1}{3!} (kr)^2 + O((kr)^4) \right) , \end{aligned} \quad (72)$$

cf. Eq. (28). The amplitude of the acoustical pressure field is $P_A \equiv \omega \rho_L A \sin(kz_0)$. Similarly, the velocity field $v(r, t)$ has an external contribution:

$$\begin{aligned} v_a(r, t) &\equiv \partial_r \phi_{in}(r, t) \\ &= \frac{P_A}{c \rho_L} \cos(\omega t) \left(\frac{\cos(kr)}{kr} - \frac{\sin(kr)}{(kr)^2} \right) = -\frac{P_A}{3c \rho_L} \cos(\omega t) \left(kr + O((kr)^3) \right) , \end{aligned} \quad (73)$$

cf. Eq. (27), which also enters our results for the bubble equation of motion and pressure boundary condition. In general, both quantities, P_a and v_a , are determined by the experimental set-up, in particular the external ultrasound sources which drive the bubble oscillations.

Finally, we rewrite the relevant spherically symmetric part of the external velocity potential as a superposition of an outgoing and an ingoing spherical wave. We obtain:

$$\phi_{in}(r, t) = \frac{c P_A}{2 \omega^2 \rho_L} \{ \sin(\omega[t + r/c]) - \sin(\omega[t - r/c]) \} / r , \quad (74)$$

which will be useful in the following section.

4.3 A Nonperturbative Bubble Equation of Motion

We present in this section the bubble equation of motion resulting when we do not use the expansion in \dot{R}/c which was employed in Section 4.1, see Ref. [3] for earlier related work.

Since the velocity potential ϕ obeys the spherical wave equation (13) for the presently considered case of a spherically symmetric gas bubble immersed in a liquid, we can immediately write down its most general form (see Section 2.2):

$$\phi(r, t) = \frac{1}{r} (f(t_{ret}) + g(t_{adv}) - g(t_{ret})) \quad , \quad (75)$$

with arbitrary functions f and g and where:

$$t_{ret} \equiv t - r/c \quad , \quad t_{adv} \equiv t + r/c \quad . \quad (76)$$

The terms involving g represent the external field, an example of which was considered in the previous section, see Eq. (74) in particular. Generally, the relative sign between the retarded and advanced contributions results from the requirement that the external field be regular at $r = 0$, i.e. the position of the center of the bubble. The term involving f presents the additional outgoing (sound) contribution to the velocity potential which is generated by the moving bubble wall.

Then, our task is to determine (or eliminate) the functions f and g such that ϕ satisfies the velocity boundary condition (15):

$$\dot{R} = \partial_r \phi|_R = -\frac{1}{cR} (c\phi + f'(t_{ret}) - g'(t_{adv}) - g'(t_{ret}))_R \quad , \quad (77)$$

where $f'(x) \equiv df(x)/dx$ etc., and where Eqs. (75), (76) were used to obtain its present form. Similarly, we rewrite the pressure boundary condition (56):

$$P_L(R) - \eta_L \frac{1}{r} \partial_r^2(r\phi)|_R = P_G(R) - (4\eta_{sL} + 3\eta_{bG}) \frac{\dot{R}}{R} - \frac{2\sigma}{R} \quad . \quad (78)$$

Here we made use of the velocity boundary condition, i.e. the first of Eqs. (77), and assumed the linear velocity profile inside the bubble which was introduced in Section 3, $v = \partial_r \phi = r\dot{R}/R$ for $r \leq R$, which determines the gas viscosity term $\propto \eta_{bG}$. As we pointed out already after Eq. (56), only the bulk viscosity of the gas contributes for a linear (homologous) velocity profile.

Furthermore, as discussed in Section 4.1, we employ the Navier-Stokes equation Eq. (53) as the underlying dynamical equation of motion of the gas and liquid fluids. Integrating over the radial coordinate r , we obtained the nonperturbative Eq. (66) before, which we presently rewrite as:

$$-\left(\partial_t \phi + \frac{1}{2}(\partial_r \phi)^2\right)_R = \mathcal{I} + h[P_L] - \frac{\eta_L}{\rho_L} \frac{1}{r} \partial_r^2(r\phi)|_R \quad , \quad (79)$$

where $h[P_L]$ denotes the liquid enthalpy evaluated in Eq. (64) and we collected terms pertaining to the bubble interior into:

$$\mathcal{I} \equiv -\frac{1}{2}R\ddot{R} + h_G[P_G] \quad , \quad (80)$$

with the gas enthalpy h_G from Eq. (61); note that $h_G = 0$ for a homogeneous density inside the bubble. We recall once again that the contribution of the bubble interior was evaluated assuming the linear velocity profile. The discussion following Eq. (66) furthermore implies that $\mathcal{I} \equiv 0$ for the case of exactly homologous bubble interior dynamics (cf. Section 3). Equations (77), (78), and (79) completely determine the bubble motion, i.e. $R(t)$, as we shall demonstrate now. To begin with, we simplify the r.h.s. of Eq. (79) by using:

$$h_L[P_L] - \frac{\eta_L}{\rho_L} \frac{1}{r} \partial_r^2(r\phi)|_R = h_L[P_L - \eta_L \frac{1}{r} \partial_r^2(r\phi)|_R] - \frac{1}{n} \frac{\eta_L}{\rho_L} \frac{1}{r} \partial_r^2(r\phi)|_R \frac{P_L - P_0 - \eta_L \frac{1}{r} \partial_r^2(r\phi)|_R}{P_0 + P_1} + \dots \quad , \quad (81)$$

which follows from Eq. (64). Neglecting the small cross term (and higher order corrections) between viscosity and compressibility of the liquid as before, we eliminate P_L and replace the argument of $h_L[\dots]$ with the help of the pressure boundary condition (78). The result is:

$$h_L[P_G(R) - (4\eta_{sL} + 3\eta_{bG})(\dot{R}/R) - (2\sigma/R)] \equiv h_L , \quad (82)$$

which we henceforth abbreviate as indicated.

In order to proceed, we calculate:

$$\begin{aligned} \partial_t \phi|_R &= \frac{1}{R} (f'(t_{ret}) + g'(t_{adv}) - g'(t_{ret}))_R \\ &= \frac{1}{R} \left(-cR\dot{R} - c\phi + 2g'(t_{adv}) \right)_R , \end{aligned} \quad (83)$$

where we used the boundary condition (77) in the second step. Inserting this result together with $\partial_r \phi|_R = \dot{R}$ and the above evaluation of h_L back into Eq. (79), we obtain:

$$c\dot{R} + \frac{c}{R}\phi|_R - \frac{2}{R}g'(t_{adv})|_R - \frac{1}{2}\dot{R}^2 = \mathcal{I} + h_L . \quad (84)$$

We have to eliminate ϕ , in order to arrive at the closed equation for $R(t)$ which we are after.

Taking the time derivative of Eq. (84), employing Eq. (83) once more, and solving the resulting equation for ϕ , one finds explicitly:

$$\frac{c}{R}\phi|_R = \frac{R}{1 + \dot{R}/c} \left(\ddot{R} \left(1 - \frac{\dot{R}}{c} \right) - \frac{c\dot{R}}{R} + \frac{\dot{R}^2}{R} - \frac{1}{c} \frac{d}{dt} (\mathcal{I} + h_L) \right) + 2\frac{g'}{R} - 2\frac{g''}{c} , \quad (85)$$

where g' stands for $g'(t_{adv})|_R$ and g'' similarly. Reinserting this result into Eq. (84) yields:

$$c\dot{R} + \frac{R}{1 + \dot{R}/c} \left(\ddot{R} \left(1 - \frac{\dot{R}}{c} \right) - \frac{c\dot{R}}{R} \left(1 - \frac{\dot{R}}{c} \right) - \frac{1}{c} \frac{d}{dt} (\mathcal{I} + h_L) \right) - \frac{2}{c}g'' - \frac{1}{2}\dot{R}^2 = \mathcal{I} + h_L , \quad (86)$$

from which equation we will derive our final results.

First of all, we obtain a perturbative equation of motion for $R(t)$ by expanding the factor $(1 + \dot{R}/c)^{-1}$ in powers of \dot{R}/c and collecting terms. Taking up to second order corrections into account, the result is:

$$\begin{aligned} & R\ddot{R} \left(1 - 2\frac{\dot{R}}{c} + 2\left(\frac{\dot{R}}{c}\right)^2 \right) + \frac{3}{2}\dot{R}^2 \left(1 - \frac{4}{3}\frac{\dot{R}}{c} + \frac{4}{3}\left(\frac{\dot{R}}{c}\right)^2 \right) - \frac{2}{c}g''(t + R/c) \\ &= \left(1 + \frac{R}{c} \left(1 - \frac{\dot{R}}{c} \right) \frac{d}{dt} \right) (\mathcal{I} + h_L) + \mathcal{O} \left((\dot{R}/c)^3 \right) . \end{aligned} \quad (87)$$

It is straightforward to calculate higher order corrections in this case, if necessary. Equation (87), when evaluated including only first order corrections in \dot{R}/c , essentially agrees with our previous perturbative result, Eq. (69). To see this, note that $d\mathcal{I}/dt$ generates a term $\propto \ddot{R}$, using Eq. (80). The third order derivative can then be eliminated similarly as between Eqs. (67)–(69).

However, a crucial difference remains in that presently we treat the external field exactly, which is represented here by the term $\propto g''$, whereas in Section 4.1 the external field was treated perturbatively on the same footing as the sound field generated by the bubble wall motion. By comparison of Eqs. (74) and (75) (the external field terms involving g) we find here explicitly:

$$-\frac{2}{c}g''(t + R/c) = \frac{P_A}{\rho_L} \sin(\omega[t + R/c]) , \quad (88)$$

for the example of an external standing plane wave pressure field discussed in Section 4.2. We remark that \dot{R}/c may vary systematically between less than about 1 ns and about 100 ns during a nonlinear oscillation cycle with bubble parameters in the SBSL regime. Neglecting this retardation in the external field term, terms related to the bubble interior, and modifications due to the realistic liquid EoS and enthalpy, Eqs. (63) and (64), which enter our derivations, we again reproduce Eqs. (9) and (10) of Ref. [4], if we truncate Eq. (87) at $O(\dot{R}/c)$.

Alternatively, instead of expanding Eq. (86), we simply multiply this equation by the denominator $1 + \dot{R}/c$ to obtain:

$$R\ddot{R}(1 - \frac{\dot{R}}{c}) + \frac{3}{2}\dot{R}^2(1 - \frac{1}{3}\frac{\dot{R}}{c}) - \frac{2}{c}(1 + \frac{\dot{R}}{c})g''(t + R/c) = (1 + \frac{\dot{R}}{c})(\mathcal{I} + h_L) + \frac{R}{c}\frac{d}{dt}(\mathcal{I} + h_L) \quad , \quad (89)$$

which presents the nonperturbative bubble equation of motion; it agrees with the result of Ref. [3] in the limit of the idealized adiabatic liquid EoS employed there and neglecting the bubble interior (except for the pressure boundary condition).

5 Numerical Results

We now turn to a numerical study of characteristic properties of a single air bubble in water at standard laboratory conditions (STP), i.e. at the ambient temperature $T = 293$ K and under the ambient pressure $P_0 = 1 \text{ atm} = 1.01325 \cdot 10^5 \text{ kg/m} \cdot \text{s}^2$. Solutions of the nonperturbative equation of motion (89) will serve as our standard, with which other results shall be compared.

The following material ‘constants’ of water (STP) will be used [2]: density $\rho_L = 10^3 \text{ kg/m}^3$, surface tension $\sigma = 0.073 \text{ kg/s}^2$ (water/air), sound velocity $c = 1481 \text{ m/s}$. This latter value is about 2% higher than the one which follows from the adiabatic water EoS (63) at STP with the parameters given in Ref. [5], $n = 7$ and $P_1 = 3 \cdot 10^8 \text{ kg/m} \cdot \text{s}^2$, which we employ in Eqs. (64), (82). The shear and bulk viscosities of water (STP) are [2]: $\eta_{sL} = 1.002 \cdot 10^{-3} \text{ kg/m} \cdot \text{s}$, $\eta_{bL} = 2.91\eta_{sL}$.

The ‘standard’ air bubble we study has an equilibrium radius $R_0 = 4 \cdot 10^{-6} \text{ m}$. The adiabatic index is $\gamma = 1.4$, characteristic of di-atomic molecules. The equilibrium radius and the particle number N in the bubble, or equilibrium gas density ρ_0 , are related through the van der Waals EoS (44) and pressure boundary condition (78) with $P_L = P_0$ (STP), which corresponds to the following set of parameters [2]: $N = 0.913 \cdot 10^{10}$, van der Waals excluded volume $\frac{4}{3}\pi a^3 = 0.041 \text{ l/mole}$, ratio of equilibrium to hard core density $\rho_0/\rho_a = 0.0023$. For the air viscosities we take [2]: $\eta_{bG} = 0.6\eta_{sG} = 1.08 \cdot 10^{-5} \text{ kg/m} \cdot \text{s}$, which indeed make a negligible contribution in the context of our study.

The applied driving sound field, cf. Section 4.2, will be chosen to oscillate with the frequency $\nu = \omega/2\pi = 26 \text{ Khz}$ in all examples. Its amplitude will be fixed at $P_A = 1.35P_0$, except when stated otherwise.

In the numerical calculations we consider the above specified parameters as prescribed constants, but keep in mind that e.g. the sound velocity and surface tension may change appreciably. The use of a constant adiabatic index has been questioned before [1], since various transport effects leading to entropy production may become important. We follow Ref. [1] in that we artificially increase all viscosities by a factor three, which has been found necessary to fit the standard Rayleigh-Plesset equation, i.e. $R(t)$, to the experimental data obtained by lightscattering methods [11, 17].

In Fig. 1 we show the full cycle of the time dependent radius $R(t)$ of the air bubble in water (full line), the bubble surface velocity $\dot{R}(t)$ (dashed line), and the sinusoidal external driving pressure $P_a(r = 0, t)$ according to Eq. (72) (overlaid full line together with zero line, arbitrary units), which coincides with the relevant long-wavelength limit. We integrated numerically the nonperturbative Eq. (89) for a homologous bubble, in which case $\mathcal{I} = 0$ according to Eq. (80). However, the gas pressure entering through Eq. (82) is evaluated here for a homogeneous bubble for the moment; we shall consider the effect of the inhomogeneity in Section 5.3. We note that on the scale of Fig. 1,

the $R(t)$ curves calculated with the other equations derived in this work or the one used before in Refs. [4, 10, 13, 15], for example, cannot be discriminated for our typical parameter set. Therefore, we will in the following pay more attention to $\dot{R}(t)$, which is much more sensitive to the differences between the various equations of motion.

5.1 Perturbative vs. Nonperturbative Equations of Motion

The equations of motion which have been used to study driven gas bubbles in liquids in the SBSL parameter regime incorporated effects of the sound emission only in the lowest order in \dot{R}/c so far, see e.g. Refs. [1, 4, 13] and further references therein. In view of the high velocities of the bubble surface reached during the collapse phase, which may reach $\dot{R}/c \approx 1$ (\equiv Mach 1), as indicated in Fig. 1, we study here how the various approximate treatments of sound damping compare to the nonperturbative Eq. (89). The bubble interior is treated here as explained in the context of Fig. 1 above. The individual sections in Fig. 2 show the surface velocity $\dot{R}(t)$ at the first bounce (left column) and the second bounce (second column) for different amplitudes of the driving pressure (top to bottom; P_A in units of P_0); the origin of the time-axis is arbitrarily chosen for the first bounce, the delay until the corresponding one for the second bounce is indicated in each case. The results are obtained from the nonperturbative equation (full line), and its lowest order in \dot{R}/c perturbative expansion (dashed line), cf. Eq. (87), respectively. In the latter case also the retardation shifting the time argument of the driving pressure term, see Eq. (88), has been neglected, in conformity with earlier work.

It is obvious from Fig. 2 that characteristic phase shifts result w.r.t. to the cycle timing set by the external driving pressure and between the first and subsequent bounce(s). Physically most important is the fact that within the perturbative treatment the maximal surface velocity during the collapse is overestimated by a considerable amount, e.g. $\approx 250 \text{ ms}^{-1}$ for the first bounce at $P_A = 1.35P_0$. This implies that the collapse is significantly less violent than has been concluded from previous theoretical treatments of the bubble dynamics. In particular, quantitative SBSL estimates derived from models which couple the perturbatively corrected Rayleigh-Plesset equation, cf. Eq. (69), to a full hydrodynamic simulation of the bubble interior may need a revision [10, 12, 15]. We are led to this conclusion also from the various other corrections to be discussed shortly.

The origin of the retardation of the first bounce in the perturbative approach is shown in Fig. 3 to be due to the neglect in the perturbative expansion of the time retardation effect. When the retardation is included as in Eq. (88), then the positions of the first perturbative and nonperturbative bounce coincide. However, the perturbative expansion including the retardation effect continues to introduce an overestimate of the collapse velocity. This is leading to a remaining phase shift of 15-20 ns between first and subsequent bounce(s), as seen in the bottom portion of Fig. 3.

5.2 Homologous vs. Homogeneous Bubble Interior

In order to demonstrate the influence of the behavior of the bubble interior on the overall dynamics of the coupled bubble-liquid system, beyond just providing the pressure resisting the collapse, we consider here how the homologous bubble description developed in Section 3 compares with the usual simpler homogeneous matter distribution model of the bubble interior.

We exploit here the presence of a fixed point ξ_* , Eq. (52), where the density remains nearly constant. Presence of this fixed point cannot be expected in general, however, we presently make this assumption based on our numerical experience with the description of homologous and adiabatic changes of the interior distributions. We can evaluate Eq. (45) conveniently integrating from ξ_*R to R . With $P_* \equiv P(\rho_*)$, see Eq. (44), which denotes the gas pressure of the corresponding homogeneous bubble, we

obtain the following approximate result for the homologous gas pressure at the bubble surface:

$$P_G(R) = P_* \left(1 - \frac{\gamma - 1}{2} \frac{(1 - \xi_*^2) \rho_* R \ddot{R}}{(1 - \rho_*/\rho_a) P_*} \right)^{\frac{\gamma}{\gamma-1}}. \quad (90)$$

Employing this expression for the gas pressure in the nonperturbative equation of motion (89), we find the results depicted in Fig. 4 (full line), where also the behavior of a homogeneous bubble (dashed line) is shown for comparison. We observe only a rather small effect on $R(t)$, except for a 1.5 ns shift of the minimum. However, similarly to the effects illustrated in Fig. 2, we find here another sizeable reduction of the maximal collapse speed ($\approx 200 \text{ ms}^{-1}$). The maximum of the gas pressure at the homologous bubble surface is reduced by about 5%, as compared to the homogeneous one, which amounts to $\approx 10^3 \text{ atm}$. However, the maximal gas density at the surface is much less affected and reaches approximately one half liquid density in our calculational example.

5.3 The Sound Field of a SBSL Bubble

As a further application of our study of the sound field imposed on and rescattered by a typical SBSL bubble we evaluate it at a given distance away from the bubble, where it can be measured by a hydrophone, which preferably should be sensitive to the highest expected sound frequencies [1, 11].

Perturbatively, it is most convenient to obtain the sound pressure using Eq. (28) or (35) in the form:

$$P(r, t) = P_a(r, t) + \frac{\tilde{R}}{r} \left(P(\tilde{R}, \tilde{t}) - P_a(\tilde{R}, \tilde{t}) \right), \quad (91)$$

where $\tilde{R} \equiv R(\tilde{t})$ and \tilde{t} can be further evaluated with the help of Eq. (24) or Eq. (25), whichever applies. The pressure difference on the r.h.s. here can then be computed easily from the solution of the perturbative equation of motion (69), cf. Section 5.1, since it is implicitly part of it.

The result at the lowest nontrivial order in \dot{R}/c is shown in Fig. 5, for $r = 1 \text{ mm}$ away from the center of the bubble. We clearly see the outgoing compression spikes riding on the sinusoidal driving pressure, which are caused by the bubble collapse and successive bounces. On the pressure scale of this figure (cutting off the first maximum) the nonperturbative result would be indistinguishable from the perturbative calculation.

We calculate the pressure field nonperturbatively beginning with Eq. (91), as before. However, we proceed in this case by using the pressure boundary condition, Eq. (78), in order to calculate $P(R, t) \equiv P_L(R)$. The term $\propto -\eta_L$, in particular, can be evaluated in the long-wavelength limit (neglecting a cross term between viscosity and compressibility) to yield $+2\omega\eta_L P_A \cos(\omega t)/(3c^2\rho_L)$, while all other terms are straightforward to obtain from the numerical solution of the nonperturbative Eq. (89); cf. the remarks explaining the calculation of Fig. 1 in Section 5.1.

In Fig. 6 we show the nonperturbative evaluation of the first sound pressure spike at $r = 1 \text{ mm}$. For comparison, also the somewhat earlier and considerably stronger spike given by the perturbative calculation, cf. Fig. 5, is shown. If we correct the calculated amplitude here for the geometric dispersion, then the pressure at $r = 0.6 \mu\text{m}$ reaches $4.5 \cdot 10^4 \text{ atm}$ at maximum. Applying the generic damping factor of 10^{-4} for the absorption of a (300 Mhz) pulse travelling 1 mm, we arrive approximately at the pressure amplitude measured experimentally for an SBSL bubble under similar conditions as assumed in our calculation [1, 11]. However, another interesting aspect here is the rise time of the sound signal, i.e. from one-half to maximum amplitude, which takes only 40 ps (decay time 260 ps). This is about two orders of magnitude below what has been resolved in the above cited experiments.

Finally, in view of the pressure spike results presented here, it seems worth while to check one of our basic assumptions, which is the linear acoustic approximation, Section 2.1. It is underlying the linear wave equation for the velocity potential, Eq. (13), which forms the basis of our study of the emitted sound field. Whereas dispersion and absorption can be incorporated in a linearized approximation,

genuinely nonlinear effects are beyond our present scope [2]. The linear approximation requires that perturbations of the ambient state of the fluid are relatively small. Employing the adiabatic liquid EoS (63) for water and considering the maximum of the pressure amplitude obtained here, see Fig. 6, we obtain a maximal compression and ratio of sound speeds:

$$\max \frac{\rho}{\rho_L} \approx 1.4 \quad , \quad \max \frac{c(\rho)}{c(\rho_L)} \approx 2.7 \quad , \quad (92)$$

respectively. Whereas the compression may appear to be quite tolerable, the temporary increase of the sound speed and its implications for the damping of the bubble motion, when the sound pulse is launched from the collapsing bubble surface, obviously deserve further study.

Furthermore, one may wonder about the behavior of the water next to the bubble surface, when it is exposed to the “cold shock” indicated by our results, i.e. several 10^4 atm pressure increase within less than 50 ps.

6 Summary, Conclusions and Outlook

The aim of our present work has been to reconsider the sound emission from the highly nonlinear, large amplitude motion of the interface between the gas inside and the liquid outside a cavitating bubble. Previous studies typically evaluated the radiated sound field in lowest order of a perturbation expansion in \dot{R}/c , i.e. valid for slow bubble wall motion as compared to the sound velocity in the liquid. Generally, it is believed that $\dot{R}(t)$ reaches up to (or even exceeds) the sound velocity for externally driven bubbles in the parameter regime where sonoluminescence is observed experimentally [1]. This necessitates a nonperturbative treatment, such as ours, cf. Section 2.2 and see Eq. (28), in particular. We anticipate that the sound signal from a nonlinearly oscillating bubble wall may provide an important additional diagnostic tool. It should reflect the essential short-time scale(s) of this motion, which vary over several orders of magnitude [4, 13], with current technology limiting the resolution in the $(100 \text{ MHz})^{-1}$ range, i.e. less than about 10 ns. This may be particularly valuable in cases where light scattering methods [11, 17] do not truly reflect the motion of a sharply defined bubble wall or are not applicable at all, such as for liquid metals [6].

We recall that based on Section 3 we describe the bubble interior using homologous profile functions for the density and velocity distributions. These allow for a more realistic study of the dynamics and particular properties of the high compression phase of strongly driven bubble oscillations, the importance of which has been shown earlier [10, 12]. Presently we employ only a simplified version of the semianalytic variational approach developed in Refs. [13, 14]. In any case, our derivation of Eq. (89) allows to incorporate easily any more precise model of the bubble interior; and it may be possible to extend this approach in order to account for the important effects of heat conductivity and mass diffusion.

Our numerical examples obtained in Section 5 employ as another approximation the homologous solutions with the usual adiabatic van der Waals EoS. These EoS become questionable when the energy density reaches the ionization regime. The dynamic behavior of the gas mixtures within a rapidly oscillating bubble, here assumed to remain that of a di-atomic gas (air), deserves further study. In parallel to the cyclic in- and outgassing from the liquid into the bubble (“rectified diffusion”), it remains to be seen whether an essential amount of liquid vaporizes at the bubble surface and recondenses during an oscillation cycle. Related effects may help to explain the observed sensitivity of sonoluminescence to experimental parameters such as temperature in particular [1, 18, 19]. In general, transport phenomena within the bubble and across the phase boundary have to be incorporated whenever the motion becomes fast compared to characteristic relaxation times τ_i , $\dot{R} \approx \Delta_i/\tau_i$, where Δ_i denotes the scale of a corresponding gradient (e.g. mass density, partial pressure, temperature,

etc.). In particular, shock waves may be launched into the bubble interior [4, 15, 16] or exterior [10], the description of which is beyond the scope of this work.

One may speculate whether or not the liquid (water) may be trapped in a metastable state w.r.t. solidification into a high-density phase (of ice) and in which form the corresponding binding energy would be released most efficiently. Presumably it stays at or close to the ambient temperature [10]. Assuming an effective sound velocity of 2000 m/s, the 300 ps mean half width of the pressure pulse obtained in Section 5.3 corresponds to a spatial shell width of $0.6 \mu\text{m}$, i.e. about the vander Waals hard core radius employed in our calculations. Near the collapsed state with $R \approx 0.6 \mu\text{m}$ such a shell contains about 10^{11} water molecules, i.e. only about an order of magnitude more particles than assumed (in the gas) inside. Furthermore, the sound pulse amplitude decreases exponentially away from the bubble surface (besides geometric dispersion $\propto 1/r$) due to absorption in the liquid [2]. Then, assuming an extremely conservative decay $\propto \exp(-\Delta r [\text{mm}]/.434)$, one immediately estimates that the energy dissipated in this first shell (proportional to square of amplitude decrease) amounts to about 3/1000 of the pulse energy. This is more than an order of magnitude times the energy emitted in the form of visible light by a SBSL bubble [1]. The small spatio-temporal extension of the region where this energy has to be dissipated, and how, definitely deserves further study. This should provide an improved starting point for the exploration of essential aspects of the violent bubble collapse which may help to elucidate the nature of sonoluminescence. We hope to come back to one or the other of these fascinating aspects of SBSL bubbles which are especially related to their sound field in our future work.

We note that while in principle the effect of a dynamic treatment of the bubble interior on the behavior of $R(t)$, which we introduced in Section 5.2 and Fig. 4, should be part of a full hydrodynamic simulation [10, 12, 15], the sound emission discussed in Section 5.1 had not been treated properly in any of the approaches prior to our work. In view of the numerical results presented in Section 5 it is obvious that the nonperturbative treatment of the emitted sound field as proposed here, which accounts for about 50% of the damping of the driven bubble oscillations, is mandatory. In particular, the standard perturbative calculations tend to overestimate the maximally reached surface velocity during the collapse phase considerably. Thus a crucial aspect of the “preparation phase” for the unknown light emission process can be described more accurately employing the nonperturbative equation of motion derived in Section 4.3, Eq. (89). This seems particularly relevant for detailed hydrodynamic studies of the bubble interior, in which the exterior has been described by the perturbative Rayleigh-Plesset equation before [4, 10, 12, 15]. Our numerical results for the nonperturbative sound pulse emitted by an air bubble in water (Section 5.3) fit qualitatively the first experimental observations reported in Refs. [1, 11]. On the other hand, as we pointed out at the end of Section 5.3, they also indicate the limitation of our present derivations. Whereas the bubble equation of motion, Eq. (89), is derived from the intrinsically nonlinear Navier-Stokes equation, in the form of Eq. (79) of Section 4.3, our considerations of the emitted sound field are based on the acoustic approximation (see Section 2.2). Therefore, we still neglect important sound absorption and dispersion effects in the liquid. Using the realistic EoS for water, Eq. (63) in Section 4.1, we indicated in Eqs. (92) the compression of the liquid and the corresponding increase in the density dependent sound velocity which are induced by the outgoing pressure spike next to the bubble surface. It seems desirable to study in the future the importance of nonlinear effects on the propagation and fate of the extremely strong sound pulse emitted.

There are published results on full hydrodynamic simulations of the coupled bubble-liquid system, which include especially the exterior fluid [16]. However, to the best of our knowledge, so far no attention has been paid to the unusual behavior of the liquid which may be caused by the pressure spike of $10^4 \dots 10^5$ atm launched from the bubble surface, independently of whether there are shock waves generated in the bubble interior or not. We obtained such amplitudes in typical examples with generic SBSL parameters, where particularly their rise time of only about 40 ps seems quite

astounding, but also reminiscent of the shortness of the SBSL light pulses.

Acknowledgement

We thank C.E. Aguiar, B. P. Barber, L. A. Crum, R. Donangelo, Y. Hama, L.M. Pimentel, I. Scott and M. VanZeeland for stimulating discussions. This research was supported in part by US-Department of Energy under Grant No. DE-FG03-95ER40937, by NSF under grant INT-9602920, by Brazil-PRONEX-41.96.0886.00 and by FAPERJ-Rio de Janeiro. One of us (HTE) would also like to thank ITP-Santa Barbara for hospitality, where this work was in part supported by NSF under grant PHY94-07194.

References

- [1] B.P. Barber, R. Hiller, R. Löfstedt, S.J. Putterman and K.R. Weninger, “Defining the Unknowns of Sonoluminescence”, *Physics Reports* **281** (1997) 65.
- [2] A. D. Pierce, *Acoustics – An Introduction to Its Physical Principles and Applications* (Acoustical Society of America, New York, 1991).
- [3] J. B. Keller and M. Miksis, “Bubble oscillations of large amplitude”, *J. Acoust. Soc. Am.* **68** (1980) 626.
- [4] R. Löfstedt, B. P. Barber and S. J. Putterman, “Toward a hydrodynamic theory of sonoluminescence”, *Phys. Fluids A* **5** (1993) 2911.
- [5] E. A. Neppiras, “Acoustic Cavitation”, *Phys. Rep.* **61** (1980) 159.
- [6] F. R. Young, *Cavitation* (McGraw-Hill, London, 1989).
- [7] C. Brennen, *Cavitation and Bubble Dynamics* (Oxford University Press, New York, 1995).
- [8] D.F. Gaitan, L.A. Crum, C.C. Church and R.A. Roy, “Sonoluminescence and Bubble Dynamics for a Single, Stable Cavitation Bubble”, *J. Acoust. Soc. Am.* **91** (1992) 3166;
D.F. Gaitan and L.A. Crum, “Sonoluminescence From Single Bubbles”, *J. Acoust. Soc. Am.*, Suppl. 1, **87**(1990) S141.
- [9] B.P. Barber and S.J. Putterman, “Observation of Synchronous Picosecond Sonoluminescence”, *Nature* **352** (1991) 318;
B.P. Barber and S.J. Putterman, “Spectrum of Synchronous Picosecond Sonoluminescence”, *Phys. Rev. Lett* **69** (1992) 1182;
B.P. Barber, “Synchronous Picosecond Sonoluminescence”, Ph.D. Thesis, Department of Physics, UCLA, Technical Report BB92 (June 1992), unpublished.
- [10] M.-C. Chu and D. Leung, “Effects of Thermal Conduction in Sonoluminescence”, *J. Phys.: Condens. Matter* **9** (1997) 3387.
- [11] K. R. Weninger, B. P. Barber, and S. J. Putterman, “Pulsed Mie Scattering Measurements of the Collapse of a Sonoluminescing Bubble”, *Phys. Rev. Lett.* **78** (1997) 1799.
- [12] M.-C. Chu, “The Homologous Contraction of a Sonoluminescing Bubble”, *Phys. Rev. Lett.* **76** (1996) 4632.
- [13] I. Scott, H.-Th. Elze, T. Kodama, and J. Rafelski, “Time Evolution and Energy Content of Cavitating Gas Bubbles”, Univ. of Arizona preprint AZPH-TH/96-28R.

- [14] T. Kodama, H.-Th. Elze, J. Rafelski and I. Scott, “Variational Description of Dynamics of Gas Bubble Cavitation”, in: Proceedings of *ECT*-Trento*, May 1997 workshop, L. Csernai et al. (eds.).
- [15] C. C. Wu and P. H. Roberts, “Shock-Wave Propagation in a Sonoluminescing Gas Bubble”, *Phys. Rev. Lett.* **70** (1993) 3424.
- [16] W. Moss, D.B. Clarke, J.W. White and D.A. Young, “Hydrodynamic Simulations of Bubble Collapse and Picosecond Sonoluminescence”, *Phys. Fluids* **6** (1994) 2979;
“Sonoluminescence and the Prospects for Table-Top Micro-Thermonuclear Fusion”, *Phys. Lett. A* **211** (1996) 69.
- [17] B. P. Barber and S. J. Putterman, “Light scattering measurements of the repetitive supersonic implosion of a sonoluminescent bubble”, *Phys. Rev. Lett.* **69** (1992) 3839.
- [18] R. Hiller, K. Wenninger, S. J. Putterman, and B. P. Barber, “Effect of Noble Gas Doping in Single-Bubble Sonoluminescence”, *Science* **266** (1994) 248.
- [19] B. P. Barber, C. C. Wu, R. Löfstedt, P. H. Roberts, and S. J. Putterman, “Sensitivity of Sonoluminescence to Experimental Parameters”, *Phys. Rev. Lett.* **72** (1994) 1380.

Figure Captions

Fig. 1 : Radius R (full line) and surface velocity \dot{R} (dashed line) as a function of time for an air bubble in water computed according to the nonperturbative Eq. (89). The time dependent driving pressure with $P_A = 1.35P_0$ is shown (overlaid together with zero line, arbitrary units). See main text for specification of other system parameters and further details.

Fig. 2 : Surface velocity $\dot{R}(t)$ for the bubble of Fig. 1 at first bounce (left column) and second bounce (second column) for different amplitudes of driving pressure (top to bottom; P_A in units of P_0); the delay between origins of the time-axes between the bounces is indicated. Results from the nonperturbative Eq. (89) (full line) and the perturbative Eq. (87) (dashed line); see main text for further details.

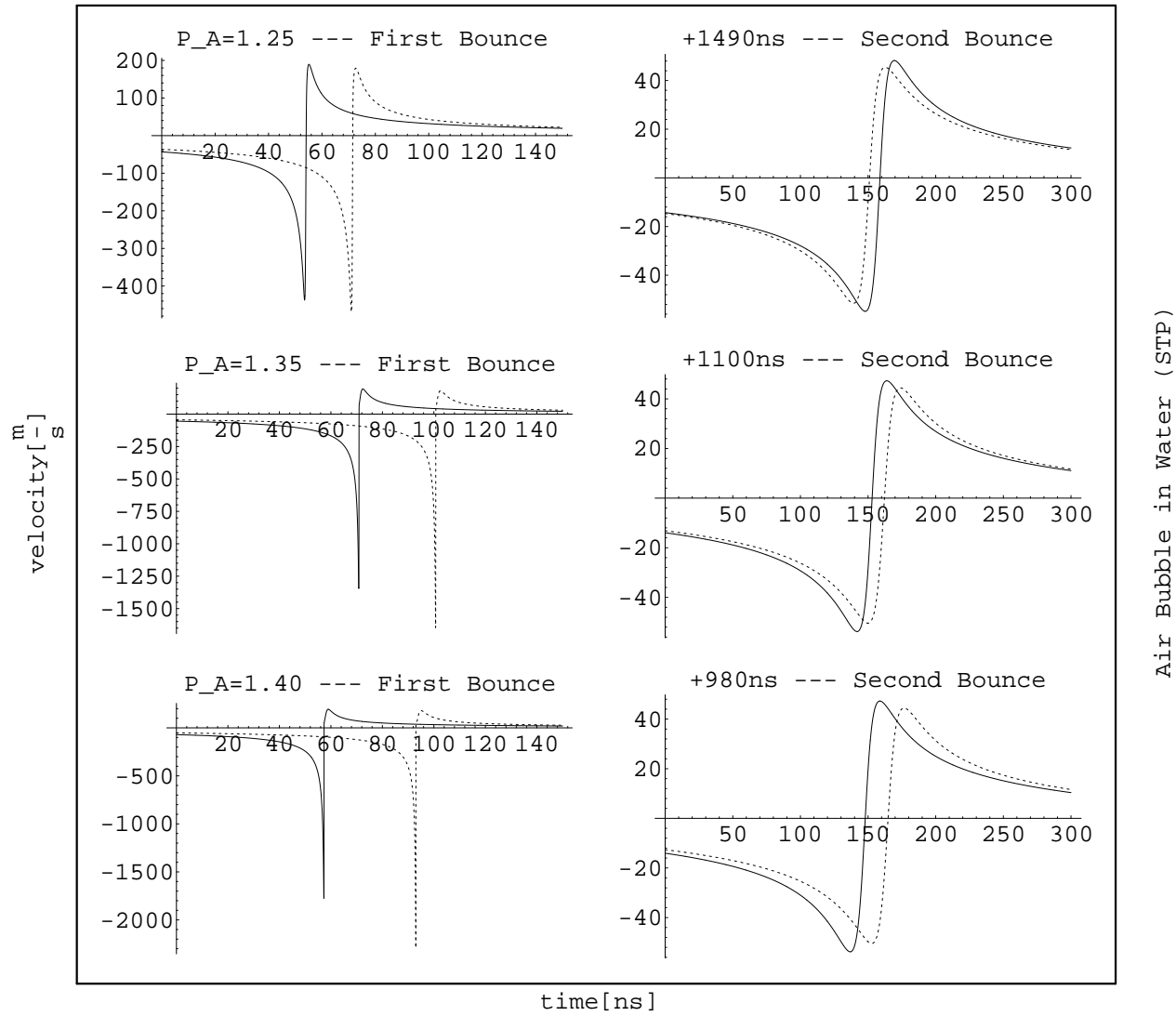
Fig. 3 : Same as Fig. 2, however, employing the nonperturbative Eq. (89) (full line) and perturbative Eq. (69), comprising time retardation (dashed line).

Fig. 4 : Comparison of the radius R (top) and surface velocity \dot{R} (bottom) for the bubble of Fig. 1, using Eq. (89), for a homologous (full line) and a homogeneous (dashed line) bubble.

Fig. 5 : The pressure amplitude at $r = 1\text{mm}$ from the center of the bubble of Fig. 1, calculation including $O(\dot{R}/c)$ corrections; see main text for further details.

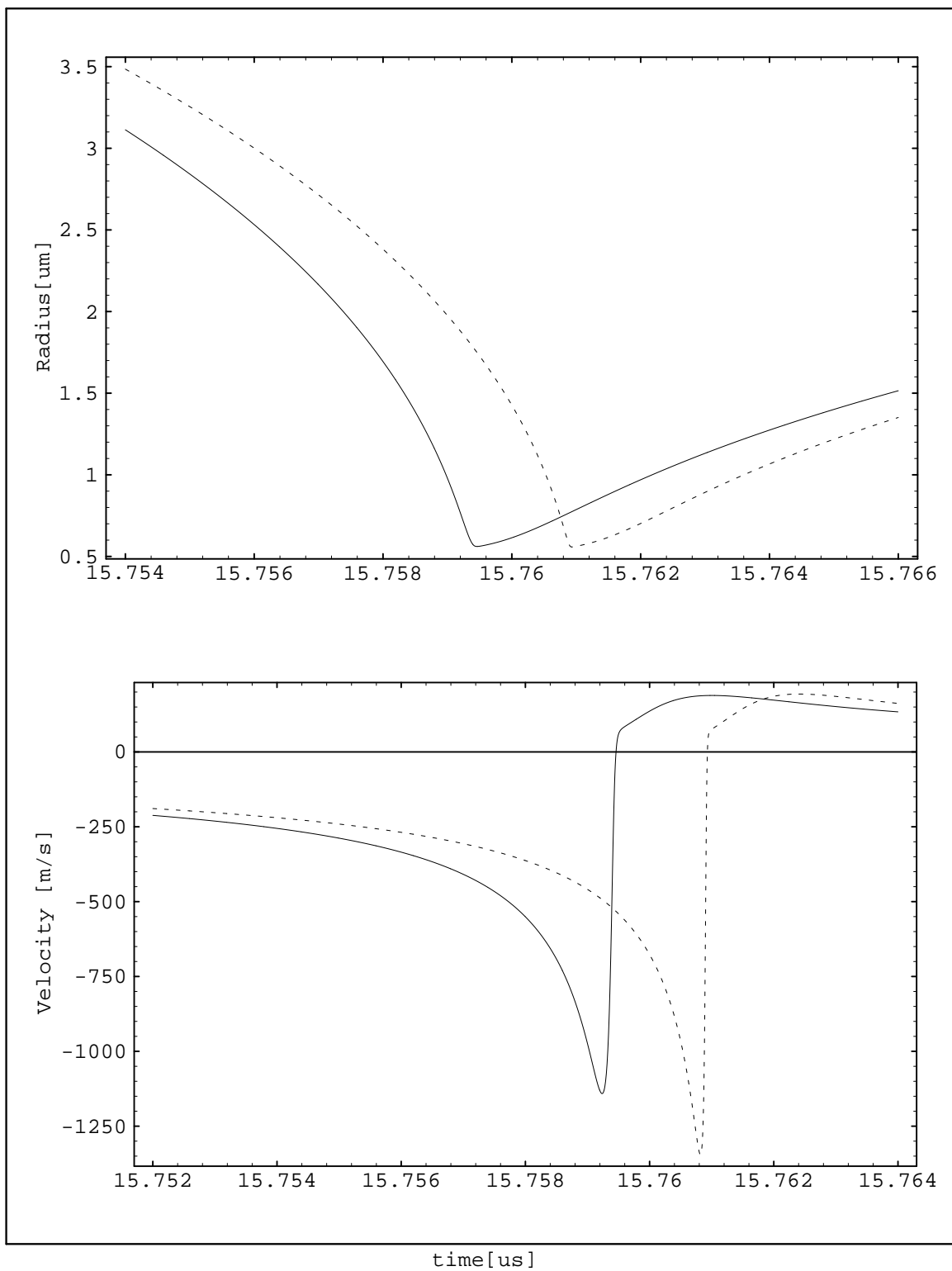
Fig. 6 : The first spike of the outgoing compression pulse launched by the collapsing bubble, see Fig. 5. For comparison the result of the nonperturbative calculation (smaller, later pulse) is shown together with the perturbative one at $O(\dot{R}/c)$.

Perturbative vs. Nonperturbative Sound Emission



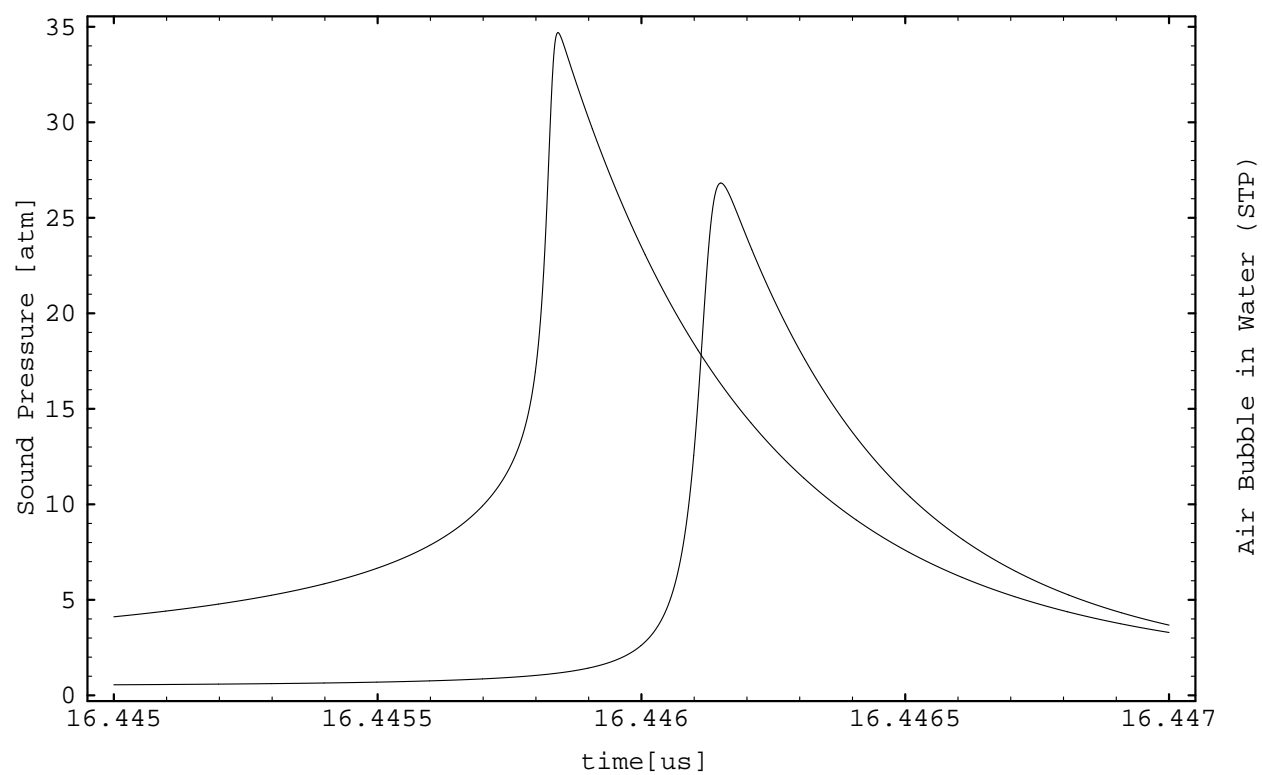
Homologous vs. Homogeneous Bubble

Bubble Characteristics

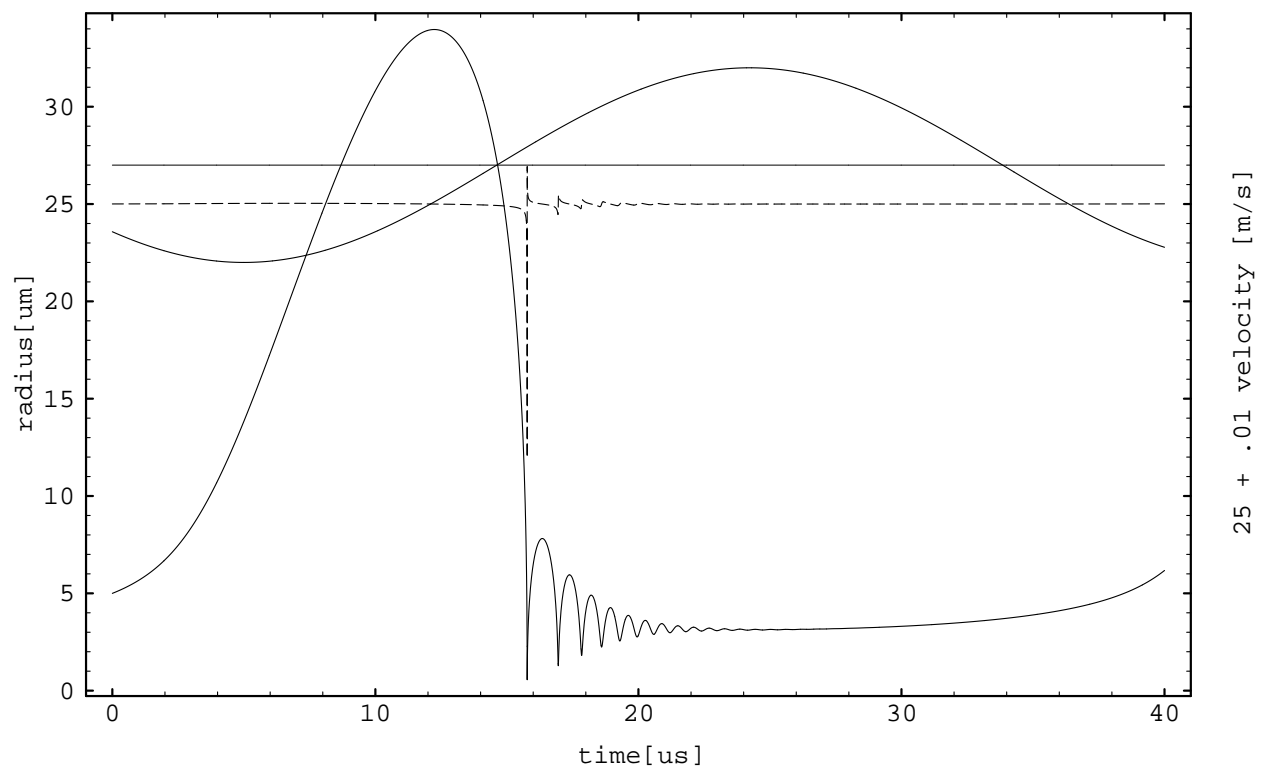


Air Bubble in Water (STP), $P_A=1.35$

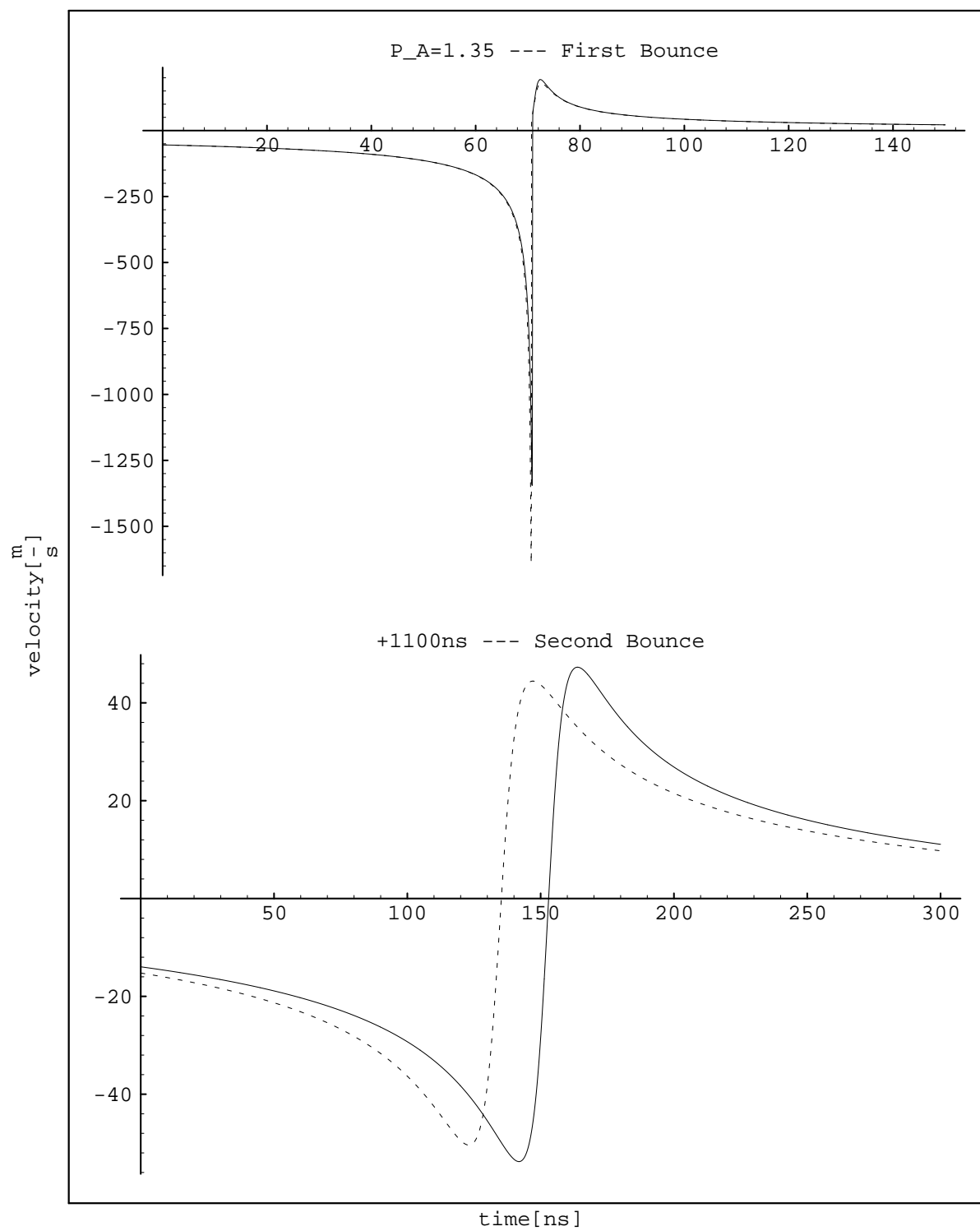
0th order vs. nonperturbative calculation, $r=1\text{mm}$, $P_A=1.35$



Air Bubble in Water (STP)



Perturbative vs. Nonperturbative Sound Emission



Air Bubble in Water (STP)

